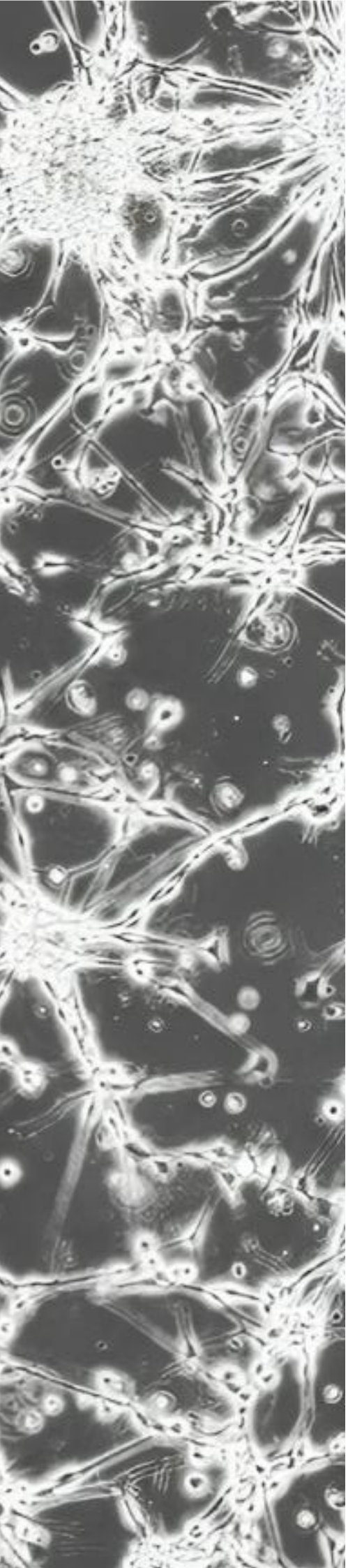

Impact of Glioblastoma Multiforme on Blood-Brain Barrier Integrity

Elaxmi Sathiyalingam

Master's Thesis

August 2024

Aalborg University
Department of Health Science and Technology
Biomedicine

AALBORG UNIVERSITY
STUDENT REPORT

Medicine with Industrial Specialisation
Biomedicin
Aalborg University
http://www.aau.dk

Title: Impact of Glioblastoma Multiforme on Blood-Brain Barrier Integrity

Theme: Glioblastoma Multiforme and Blood-Brain Barrier

Project Period: September 1st 2023 – August 14th 2024

Project Group: 9023

ECTS: 60 points

Participant(s): Elaxmi Sathiyalingam

Supervisor: Louiza Bohn Thomsen, Ph.D., Associate Professor

Project Technicians: Hanne Krone Nielsen and Merete Fredsgaard

Page Numbers: 61

Date of Completion: 14th August 2024

S. Elaxmi

Author

Preface

The master's thesis was conducted at the Department of Health Science and Technology at Aalborg University from September 2023 to August 2024. References appear as (Surname, Year) according to the Harvard citation style. A citation places before the dot refers to the sentence whereas after the dot refers to the entire section. All figures are created in BioRender and the statistical graphs are made in GraphPad.

Acknowledgements

First and foremost, I would like to thank my supervisor, Louiza Bohn Thomsen, for their unlimited support, precious guidance and endless optimism and encouragement throughout the thesis, especially during the challenging moments in the laboratory. Your knowledge and patience were invaluable in aiding me guide through the challenges that have occurred throughout this thesis. Lastly, I would like to thank her for the tips and advice that I have received during the writing process.

Furthermore, I would like to thank all the laboratory technicians, especially Merete Fredsgaard, Hanne Krone Nielsen, Ditte Bech Laursen and Brita Holst Serup. Your technical expertise and help in the laboratory work was instrumental in the completion of my experiments.

I want to show my appreciation to the Medical Microbiology and Immunology group for letting me be a part of the team throughout this year and for all the scientific discussions during the meetings. I want to express my gratitude to Trine Søndergaard Jensen and Natasja Bruun for their insightful advice and willingness to help and share their experiences and knowledge along with the many wonderful conversations throughout this year.

Lastly, I would like to thank my fellow classmates, Karoline Vadskær Andersen and Frederik Hegner Odgaard. Our shared experiences, friendship and encouragement has made this journey invaluable. The countless conversations and laboratory sessions made the challenges throughout this thesis more manageable and meaningful.

I am truly grateful to have experienced this academic journey with all of these wonderful individuals.

Abstract

Background: GBM is the most malignant form of brain tumour with mean survival time of around 14 to 18 months after diagnosis. The presence of a tumour affects the integrity of the BBB, changing it into the BBTB. The alteration to BBTB involves various changes, including downregulation of tight junctions, increased angiogenesis and upregulation of efflux transporters, causing a concern in the delivery of drugs through the barrier.

Aim: This thesis aims to investigate the two GBM associated cell lines, T10 and U87, and their effect on the BBB's integrity.

Methods: This thesis utilised two GBM associated cell lines, T10 and U87. *In vitro* barrier models were utilised to set up three set-ups, including a monoculture with PBCECs, co-culture with T10 and co-culture with U87. RT-qPCR was performed from the samples obtained from the three barrier models to investigate the expression of claudin-5, ZO-1, TfR, VEGFR1, P-gp and LRP1. In addition, an RT-qPCR was done to investigate the two GBM associated cell lines, T10 and U87, to examine the expression of EGFR, VEGF-A, COX-2 and Ang-2. ICC was performed on the barrier models with the different set-ups as well to investigate the expression of claudin-5 visually. Lastly, an IHC was performed on murine brain sections with T10 to investigate the expression of claudin-5, VEGFR1 and P-gp visually.

Results and discussion: The results indicate that the TEER values of the co-culture with T10 were significantly higher than the control with only PBCECs. The TEER values of the co-culture with U87 showed significant decrease at certain timestamps. The RT-qPCR of the barrier models indicate that there were significant differences in claudin-5, VEGFR1, P-gp and LRP1 in between the three set-ups. The relative gene expression of the GBM associated cancer cell showed that T10 had significantly lower expression of EGFR, VEGF-A and COX-2 compared to U87. The ICC and IHC stainings confirmed presence of claudin-5, VEGFR1 and P-gp in their corresponding stainings. Existing literature has observed differences in the mentioned markers; however, this requires further investigation due to cancer's heterogeneity.

Conclusion: Based of the findings in this thesis, further investigation is necessary in understanding the GBM associated cell lines, T10 and U87, as their heterogeneity caused variety in the integrity of the BBB.

List of Abbreviations

ABC	ATP-binding cassette
AMT	Adsorptive-mediated transcytosis
Ang-2	Angiopoietin-2
BBB	Blood-brain barrier
BBTB	Blood-brain tumour barrier
BCECs	Brain capillary endothelial cells
BCRP	Breast cancer resistance protein
bFGF	Basic fibroblast growth factor
BSA	Bovine serum albumin
CMT	Carrier-mediated transcytosis
CNS	Central nervous system
COX-2	Cyclooxygenase-2
DAPI	4′,6-diamidino-2-phenylindole
DNA	Deoxyribonucleic acid
EGFR	Epidermal growth factor receptor
FCS	Fetal calf serum
FGF-2	Fibroblast growth factor 2
GBM	Glioblastoma multiforme
ICC	Immunocytochemistry
IDH1	Isocitrate dehydrogenase 1
IHC	Immunohistochemistry
ITS	Insulin-transferrin-selenium
KPBS	Potassium phosphate buffered saline
LRP1	Low-density lipoprotein receptor-related receptor 1
MAGUK	Membrane-associated guanylate kinase
MDR	Multi drug resistance
NTC	No template control
PBCECs	Porcine brain capillary endothelial cells
PBS	Phosphate buffered saline
PDS	Plasma derived bovine serum
P-gp	P-glycoprotein
PI3K/AKT	Phosphoinositide 3-kinase/protein kinase B
RGE	Relative gene expression
RMT	Receptor-mediated transcytosis
RNA	Ribonucleic acid
RT-	Reverse transcriptase
RT-qPCR	Reverse transcription-quantitative polymerase chain reaction
TEER	Trans-endothelial electrical resistance
TfR	Transferrin receptor
TJs	Tight junctions
TME	Tumour microenvironment
TMZ	Temozolomide
VEGF	Vascular endothelial growth factor
VEGFR1	Vascular endothelial growth factor receptor 1
WHO	World Health Organization
ZO	Zonula occludens

Contents

1. Introduction

1.1 Glioblastoma Multiforme

The classification of brain tumours is based on the histological features and biological characteristics. Brain tumours can be divided into two main categories: primary tumours, which originate in the brain, and secondary tumours that metastasise to the brain from other parts of the body (Hanif et al., 2017). The World Health Organization (WHO) grades brain tumours from I to IV, with higher grades corresponding to high aggression and malignant behaviour (*see table 1*) (Hanif et al., 2017).

Table 1: An overview of the WHO classifications of brain tumours. The table includes the various grades of brain tumours with their associated name and characteristics (Kleihues et al., 1995).

Grade	Name	Characteristics
I	Pilocytic Astrocytoma	Slow growth, low proliferation and well-defined borders
II	Diffuse Astrocytoma	Infiltrative, diffuse, low mitotic activity and can progress to higher grade tumour
III	Anaplastic Astrocytoma	Infiltrative, increased mitotic activity and can progress to higher grade tumour
IV	Glioblastoma Multiforme	Vascular proliferation, high invasion, necrosis and high mitotic activity

Glioblastoma multiforme (GBM) is the most malignant form of brain tumour, which represents 77-81% of all primary tumours in the central nervous system (CNS) (Kleihues et al., 1995, Hanif et al., 2017, Grech et al., 2020). The incidence of GBM is higher in men compared to women and affects Caucasians more than any other ethnicity (Hanif et al., 2017, Wu, W. et al., 2021). The disease has a very poor prognosis, and patients have a mean survival time of around 14 to 18 months after diagnosis (Hanif et al., 2017, Grech et al., 2020, Rajaratnam et al., 2020). GBM is characterised by various factors including rapid growth, infiltrative, heterogeneity, anaplasia, increased angiogenesis, necrosis and uncontrolled proliferation (Kleihues et al., 1995, Jovčevska, Kočevar & Komel, 2013, Rajaratnam et al., 2020, Kesari, 2011).

1.1.1 Pathogenesis

The pathogenesis of GBM involves both genetic and molecular alterations, which leads to its malignancy (*see figure 1*). GBM originates from astrocytes, which are essential for supporting and protecting the neurons in the brain (Kleihues et al., 1995, Hanif et al., 2017). GBM can be classified into primary *de novo* or secondary (Kleihues et al., 1995, Wu, W. et al., 2021). Primary GBM comprises 90% of the cases, whereas the occurrence

of secondary GBM is due to progression from a lower-grade astrocytoma, which typically affects younger patients (Kesari, 2011).

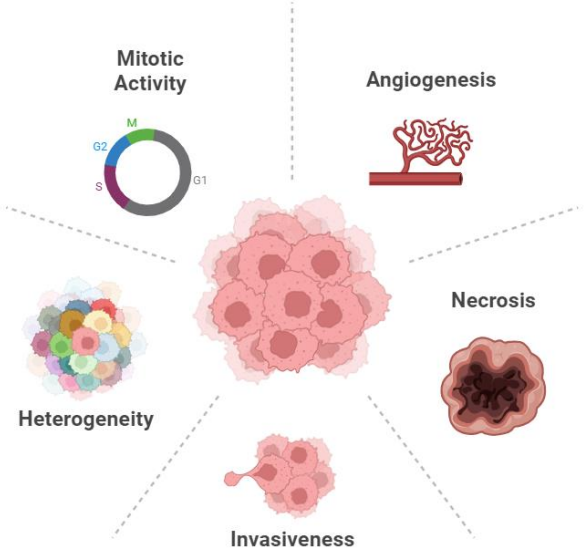

Figure 1: An overview of the various Hallmarks in Glioblastoma Multiforme. This includes the following: angiogenesis, necrosis, invasiveness, heterogeneity and mitotic activity. Inspired by (Kleihues et al., 1995, Jovčevska, Kočevar & Komel, 2013, Rajaratnam et al., 2020, Kesari, 2011). Created in BioRender.com.

Genetic alterations play a crucial impact in the progression and development of GBM. Epidermal growth factor receptor (EGFR) has been found in various forms of cancer, especially GBM, in which 40% have shown an amplification of the EGFR gene (Kesari, 2011, Wu, W. et al., 2021). This results in the increased proliferation, invasion and cell survival of cancer cells (Kesari, 2011). Additionally, isocitrate dehydrogenase 1 (IDH1) has been implicated to have a role in cancer, but it occurs mainly in secondary GBM (Rajaratnam et al., 2020). Lastly, mutations in the tumour suppressor genes, e.g., PTEN and TP53, are prevalent in GBM (Wu, W. et al., 2021). Loss of PTEN results in the activation of phosphoinositide 3-kinase/protein kinase B (PI3K/AKT) pathway, which is associated with resistance to apoptosis, increased proliferation, invasion and survival (Wu, W. et al., 2021, Rajaratnam et al., 2020, Hashemi et al., 2023). TP53 mutations lead to the loss of cell cycle control and cellular homeostasis (Zhang, Y. et al., 2018). Altogether, these different alterations contribute to GBM's characteristics (*see figure 1*).

In addition, the tumour microenvironment (TME) also has a key role in the pathogenesis of GBM (Sharma et al., 2023). The tumour cells interact with the different components of the microenvironment such as endothelial cells, astrocytes, neurons, oligodendrocytes and immune cells (Sharma et al., 2023). TME facilitates various pro-tumourigenic

mechanisms, e.g., angiogenesis, migration and proliferation (Sharma et al., 2023). Moreover, the hypoxic environment in GBM upregulates the expression of pro-angiogenic genes including vascular endothelial growth factor (VEGF) and angiopoietin-2 (Ang-2), which also leads to an increase of angiogenesis, tumour migration and invasion (Sharma et al., 2023, Koga et al., 2001). Regarding Ang-2, it is discovered on endothelial cells and glioma cells, in which it is mostly expressed near necrotic areas and the periphery of the GBM (Koga et al., 2001). Lastly, another gene that is upregulated in glioma cells is cyclooxygenase-2 (COX-2), which also is expressed near necrotic and peripheral regions of GBM (Qiu, Shi & Jiang, 2017). COX-2 is, however, poorly expressed in surrounding healthy tissues indicating that the hypoxic microenvironment is a factor in the increase of COX-2 in GBM (Qiu, Shi & Jiang, 2017).

1.1.2 Clinical Treatment

The treatment of GBM involves a combination of surgery, chemotherapy and radiation therapy (Hanif et al., 2017, Wu, W. et al., 2021, Rajaratnam et al., 2020, Jovčevska, Kočevar & Komel, 2013). Regardless of the advanced treatment options, the prognosis remains poor for GBM. The first line treatment of GBM is surgery, in which the goal is to safely resect the tumour and thereby relieve the pressure in the brain and reduce symptoms but also prolong the overall survival rate (Wu, W. et al., 2021, Rajaratnam et al., 2020). However, complete resection of the tumour is difficult due to GBM's invasiveness, which infiltrates the surrounding brain tissue (Seker-Polat et al., 2022). Both magnetic resonance imaging and intraoperative fluorescence imaging, which commonly involves 5-aminolevulinic acid, can help to locate the tumour easier for resection due to its ability to accumulate in cancer cells (Wu, W. et al., 2021).

Surgical removal is followed by radiation therapy over six weeks, which targets the residual tumour cells while leaving the healthy brain tissue intact resulting in the minimisation of possible side effects (Wu, W. et al., 2021, Rajaratnam et al., 2020). This includes techniques such as conformal radiation therapy and stereotaxic radiosurgery (Wu, W. et al., 2021, Rajaratnam et al., 2020). Additionally, chemotherapy is used concurrently with radiation therapy. The standard chemotherapeutic drug for GBM is temozolomide (TMZ). It is a small alkylating agent, which directly impairs the tumour cells by methylating the DNA resulting in apoptosis (Wu, W. et al., 2021, Rajaratnam et al., 2020, Jovčevska, Kočevar & Komel, 2013). The DNA repair protein, methyl guanine

methyl transferase, results in a reduced TMZ response by counteracting its effect (Grech et al., 2020, Wu, W. et al., 2021).

All in all, GBM is difficult to treat due to its aggressiveness and invasiveness along with lack of treatment choices. Nonetheless, it is not the only challenge in the treatment as the presence of the blood-brain barrier (BBB) complicates the delivery of drugs to the brain.

1.2 The Blood-Brain Barrier

The BBB is a highly specialised selective barrier, which separates the CNS from the peripheral circulation. It plays an important role in maintaining the homeostasis of the CNS by regulating the entry of toxins and substances into the brain (Wu, D. et al., 2023). The first discovery of the existence of the BBB was done by Ehrlich in 1885 by intravenously injecting trypan blue dye, which stained all tissue besides the brain (Ehrlich, 1885). This discovery has led to significant research of the BBB both physiologically and biologically.

The BBB is composed of non-fenestrated brain capillary endothelial cells (BCECs), which are supported by pericytes and astrocytes (*see figure 2*) (Daneman, Prat, 2015, Thomsen, M. S. et al., 2021). Both pericytes and astrocytes are essential to maintain the integrity and function of BBB (Brown et al., 2019, Kwon, Koh, 2020). Pericytes provide physiological/structural support and regulate cerebral blood flow (Brown et al., 2019), while astrocytes provide growth factors to neurons, regulate cerebral blood flow and regulate extracellular balance of e.g., transmitters and ions (Kwon, Koh, 2020).

The BCECs differ from the peripheral endothelial cells as they have specific characteristics such as the presence of tight junctions (TJs) and adherens junctions, which limits the paracellular transport of various substances from the peripheral blood to the brain (Wu, D. et al., 2023). Additionally, the BCECs contain low fenestration, high metabolic activity and limited transcytosis, which altogether restrict transcellular transport from the peripheral blood to the brain (Wu, D. et al., 2023, Burkhart et al., 2015). The complex interplay between the various cell types of the BBB along with its functioning properties appoints the BBB a protective organ for the brain.

However, the impermeability of the BBB causes a major challenge in the delivery of therapeutic drugs since only lipophilic molecules of the size 400 Da or smaller can passage

through to the brain (Pardridge, William M., 2005). Resulting in an obstacle in the treatment of neurological diseases such as GBM.

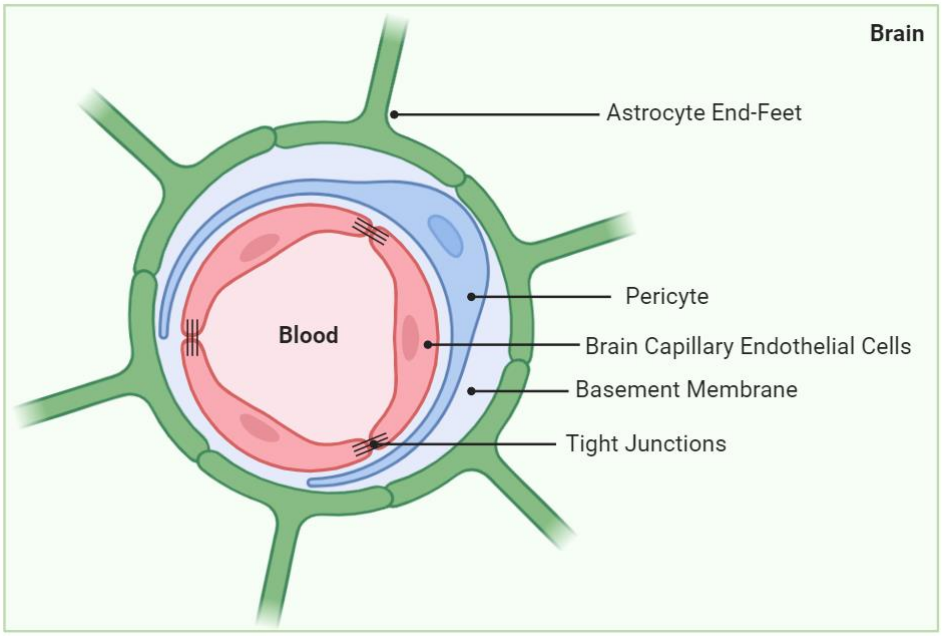

Figure 2: An overview of the Blood-Brain Barrier (BBB). Cross-section of the BBB structure including the following elements: brain capillary endothelial cells connected by tight junctions surrounded by a pericyte in the basement membrane, which is encircled by astrocytic end-feet. Inspired by (Wu, D. et al., 2023, Kaya, Ahishali, 2021). Created in BioRender.com.

1.2.1 Tight Junctions

The spaces between the BCECs are sealed by unique TJs. Compared to the ones in the peripheral capillaries, these are 50-100 times closer resulting in the restriction of passive diffusion of substances to the brain (Wu, D. et al., 2023, Profaci et al., 2020). Additionally, TJs also cause the blood vessels to have particularly high trans-endothelial electrical resistance (TEER), which adds to their ability to maintain homeostasis of the BBB (Wu, D. et al., 2023, Profaci et al., 2020). TJs are composed of transmembrane proteins, e.g., claudin and occludin, which are attached to an actin cytoskeleton through cytoplasmatic accessory proteins, e.g., the zonula occludens (ZO) family (Neyrinck-Leglantier et al., 2021, Wu, D. et al., 2023). This interaction causes the TJs to have their stability and sealing properties, which ensures the safety and normal functionality of the BBB (Kaya, Ahishali, 2021).

1.2.1.1 Claudin-5

Claudin consists of a multigene family with 27 members, however, mainly claudin-1, -3, -5 and likely -12 are expressed in the BBB (Bauer et al., 2014). This thesis will only focus on claudin-5. Claudin-5 has been observed in various tissues in human such as intestines,

lung and exocrine, however, it is expressed abundantly in BCECs and 100 times greater than any other claudin (Brunner et al., 2020). Unlike any other place in the human body, claudin-5 causes the strongest barrier in the BCECs and thereby plays an essential role in maintaining the integrity of the BBB (Brunner et al., 2020).

Disruptions in claudin-5 expression levels can cause significant alterations in the integrity and function of BBB. In a study, the deletion of claudin-5 resulted in size-selective loosening of the BBB in mice, where molecules of the size of <800 Da could pass through (Brunner et al., 2020, Nitta et al., 2003). In contrast, the overexpression of claudin-5 results in the increase of paracellular tightness in cultured BCECs (Ohtsuki et al., 2007). Additionally, it has been shown that in the presence of GBM, claudin-5 is downregulated (Karnati et al., 2014). These studies indicate that claudin-5 has an important role in the formation of functional TJs in the BBB.

1.2.1.2 Zonula Occludens 1

The ZO family consists of three members being ZO-1, -2 and -3, which belong to the membrane-associated guanylate kinase homologs (MAGUK) family (Neyrinck-Leglantier et al., 2021). The ZO proteins consist of three PDZ domains, one SH3 domain and a guanylyl-kinase domain (Liu et al., 2012, Stevenson et al., 1986). The ZO proteins serve a crucial function in connecting transmembrane proteins to an actin cytoskeleton through its C-terminus (Liu et al., 2012). Moreover, the ZO proteins are also involved in transcriptional modulation and signal transduction (Liu et al., 2012). This thesis will focus on ZO-1.

Out of the three MAGUK proteins, ZO-1 was the first to be associated with TJs (Stevenson et al., 1986). ZO-1 is expressed in epithelial and endothelial cells along with various cells that do not have TJs (Howarth, Hughes & Stevenson, 1992). The various domains of ZO-1 are responsible for the connections between the different TJ proteins (Liu et al., 2012). Through the PDZ-1 domain, ZO-1 is connected to the C-terminus of claudin-5 whereas the PDZ-2 and -3 domains are connected to C-terminus of JAM proteins (Liu et al., 2012). Lastly, the GK domain is connected to the C-terminus of occludin (Liu et al., 2012). This interaction is critical in the stability and function of TJs (Liu et al., 2012). On the contrary, the detachment of ZO-1 from the junctional complex can lead to an increased permeability of the BBB (Fischer et al., 2002). Reduced ZO-1 levels are associated with various types of cancer that result in the loss of TJ integrity (Zhang, X. et al., 2019). This may allow free

diffusion of different nutrients that could potentially increase the survival and growth of cancer cells.

1.2.2 Transporters

As mentioned, the function of the BBB is to maintain homeostasis by excluding the entry of toxic substances and supplementing the brain with necessary nutrients e.g., glucose, proteins and peptides (Knox et al., 2022). There are a limited number of solutes that do not require transport receptors to cross the BBB such as gases (e.g., oxygen and carbon dioxide) and small lipid-soluble molecules (<400 Da) (Knox et al., 2022). Furthermore, the BBB has specific transporters, which strictly regulate the passage of molecules (Keaney, Campbell, 2015). The transporters consist of the following: passive diffusion, paracellular transport, carrier-mediated transcytosis (CMT), receptor-mediated transcytosis (RMT), adsorptive-mediated transcytosis (AMT) and efflux transport (*see figure 3*) (Georgieva, Hoekstra & Zuhorn, 2014).

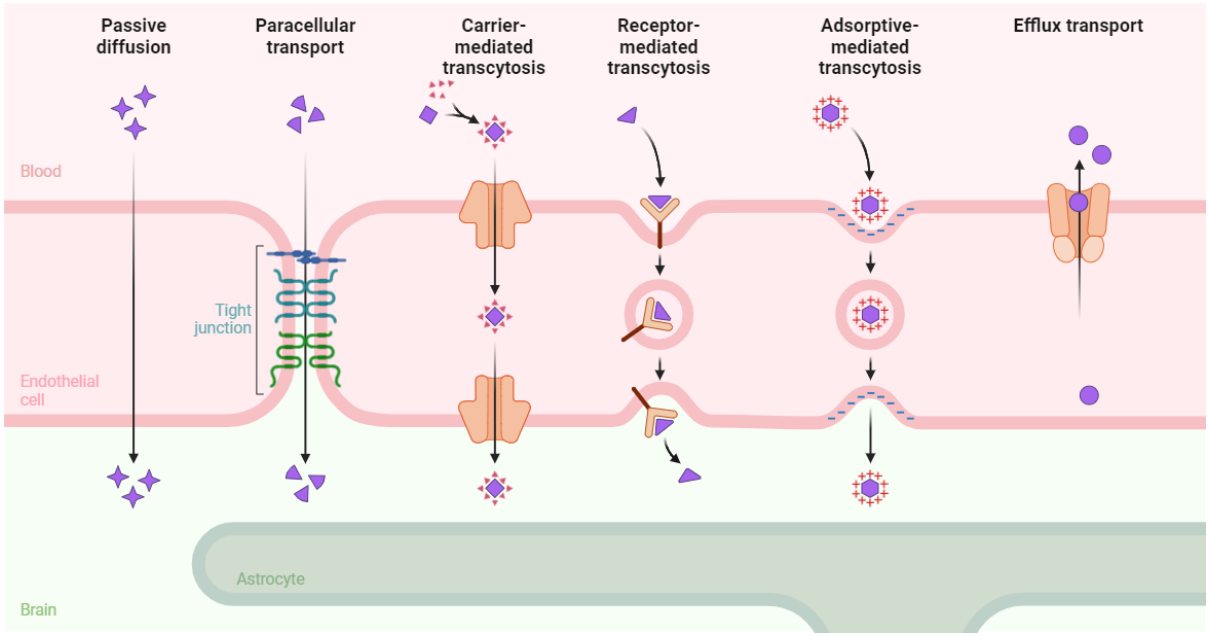

Figure 3: An overview of the various transport pathways in the blood-brain barrier (BBB). This figure contains the following transporters (from left to right): passive diffusion, paracellular transport, carrier-mediated transcytosis, receptor-mediated transcytosis, adsorptive-mediated transcytosis and lastly, efflux transport. Inspired by (Wu, D. et al., 2023, Kaya, Ahishali, 2021, Georgieva, Hoekstra & Zuhorn, 2014, Knox et al., 2022, Rathi et al., 2022). Created in BioRender.com.

Paracellular transport involves the passage of water-soluble molecules through the intercellular spacing between the BCECs. This passage is restricted due to the presence of TJs, which limits it to small molecules only. (Knox et al., 2022)

CMT is responsible for the transport of various substances through the specific carrier proteins embedded on the BCECs, however, they can also be bi-directional (Knox et al., 2022). The substances include glucose, carbohydrates, amino acids, hormones and other small metabolites (Sweeney et al., 2019). Examples of CMT involve glucose carrier 1 and choline transporter like-protein 1 (Knox et al., 2022, Sweeney et al., 2019). These substances are necessary to maintain proper brain function. However, larger molecules including transferrin, low-density-lipoprotein, insulin are transported through the BBB via RMT (Knox et al., 2022, Sweeney et al., 2019). RMT occurs through the receptor-mediated endocytosis of a substance on the luminal side, which undergoes the passage through the endothelial cytoplasm and lastly, enters the brain on the abluminal side of the BCECs through exocytosis (Knox et al., 2022, Sweeney et al., 2019). Examples of RMT include transferrin receptor (TfR) and low-density lipoprotein receptor-related receptor 1 (LRP1) (Knox et al., 2022, Sweeney et al., 2019).

AMT involves the electrostatic interaction between the negatively charged cell membrane of BCECs and the positively charged molecules, which makes it a necessary target for potential delivery of positively charged drugs (Hervé, Ghinea & Scherrmann, 2008, Song et al., 2021). The pathway of AMT is unidirectional from blood to brain, and examples of molecules using this pathway include albumin and cationic lipids (Song et al., 2021, Pulgar, 2019). Efflux transporters are responsible for exporting harmful substances and waste products from the brain into the bloodstream, which prevents the accumulation of toxic compounds within the CNS (Pardridge, William M., 2012, Knox et al., 2022). In addition, most drugs are transported out of the BCECs by efflux transporters, which limits the delivery of drugs across the BBB (Sweeney et al., 2019). The best-known efflux transporters include P-glycoprotein (P-gp) and breast cancer resistance protein (BCRP) (Sweeney et al., 2019).

1.2.2.1 Transferrin Receptor 1

TfR is a transmembrane glycoprotein that plays an important role in the cellular uptake of iron that is bound to transferrin (Johnsen et al., 2019, Pardridge, W. M., Eisenberg & Yang, 1987). Iron is necessary for many metabolic processes such as transport of oxygen, DNA synthesis and cell division (Pardridge, W. M., Eisenberg & Yang, 1987). Two different kinds of TfR have been discovered, which are referred to as TfR 1 and TfR 2 (Johnsen et al., 2019). TfR 2 is primarily expressed in tissues that regulate iron metabolism e.g., small intestines and liver, whereas TfR 1 is mostly found on the surface of many body

cells (Johnsen et al., 2019). The transport mechanism that TfR uses in BCECs is RMT (Pardridge, W. M., Eisenberg & Yang, 1987).

In addition to iron supply, the level of TfR expression is influenced by the rate of cell proliferation (Johnsen et al., 2019). Therefore, maintenance of the iron uptake is a very essential process since excess or insufficient amounts of iron within the CNS mainly is associated with neurological diseases (Johnsen et al., 2019). TfR 1 is known to be overexpressed on cancer cells due to their amplified requirement for iron in DNA synthesis allowing the rapid division of cancer cells (Guo, Z. et al., 2021). Especially in GBM, studies have shown that there is a high expression of TfR 1 (Ni et al., 2020). Therefore, TfR 1 is a well-known target for the specific delivery of drugs to the brain due to its elevated expression (Ni et al., 2020, Johnsen et al., 2019).

1.2.2.2 Vascular Endothelial Growth Factor Receptor 1

Vascular endothelial growth factor receptor 1 (VEGFR1) is a part of the VEGFR family, which consists of VEGFR1, -2 and -3 (Imoukhuede, Popel, 2012). VEGFR1 binds to VEGF A, -B and placental growth factor (Atzori et al., 2017). It is greatly expressed in vascular endothelial cells and plays an important role in angiogenesis (Amano et al., 2015). Additionally, VEGFR1 is also expressed in hematopoietic stem cells, inflammatory cells, e.g., macrophages and monocytes, and cancer metastasis (Amano et al., 2015). In the presence of tumours, VEGFR1 induces chemoresistance, inhibits apoptosis and predicts poor prognosis as well as recurrence (Atzori et al., 2017). A study by Baumgarten showed that the expression of VEGFR1 was highest in GBM and WHO grade I tumours compared to WHO grade II and III (Atzori et al., 2017, Baumgarten et al., 2016). In addition, the expression of VEGFR1 was significantly higher in the centre of the tumour (Baumgarten et al., 2016). In GBM, there is an upregulation of VEGFR1 and this activation of VEGFR1 plays a role in promoting tumour cell invasion and migration (Atzori et al., 2018). It supports that the upregulation of VEGFR1 in GBM compromises the BBB integrity and adds to the importance of investigating VEGFR1 further.

1.2.2.3 P-glycoprotein

P-gp, also known as multi drug resistance (MDR) 1 or ATP-binding cassette (ABC) sub-family B member 1, is a glycoprotein and member of the ABC transporter family (Chai, Callaghan & Gelissen, 2022, Dréan et al., 2018). It is a protein that is highly expressed on the BCECs and functions in protecting the brain by removing toxic substances from the brain to the peripheral blood (Dréan et al., 2018, Aryal et al., 2017, van Assema et al.,

2012). P-gp is known for its role in MDR, especially in cancer cells, since it can pump out the chemotherapeutic drugs resulting in a reduced efficacy (Aryal et al., 2017). As mentioned previously, the main efflux transporters in the BBB include P-gp and BCRP, which both often are upregulated in GBM (Dréan et al., 2018, Aryal et al., 2017).

Reduced P-gp has been linked to a greater exposure to toxic substances, whereas upregulated P-gp plays role in greater protection, which is observed in brain tumours, contributing to the failure of pharmacotherapeutic drugs (Chai, Callaghan & Gelissen, 2022). Not only do the BCECs express P-gp but also the cancer cells, which can result in tumours developing resistance towards the various therapeutics (Aryal et al., 2017). Using P-gp as a potential target could enhance drug retention in cancer cells and improve the therapeutic outcomes for patients with GBM.

1.2.2.4 Low-Density Lipoprotein Receptor-Related Receptor 1

LRP1 is a part of the low-density lipoprotein receptor family, which is mainly found in liver but also expressed in the brain (Zhao et al., 2016). This receptor has various physiological functions including cellular signalling and endocytosis, which both are necessary in numerous biological processes e.g., lipid metabolism, tissue invasion, cell growth and cell differentiation (Boucher, P., Herz, 2011). In the CNS, LRP1 is prominently expressed in neurons, vascular cells and glial cells where it plays an essential role in maintaining homeostasis and the structural integrity of the BBB (Kanekiyo, Bu, 2014).

An essential nutrient that LRP1 is responsible for importing into the BBB is cholesterol whereas it is exported from the brain through ABC transporters (Shruthi et al., 2022). Cholesterol is necessary due to its role in normal brain development and the brain is also the most cholesterol-rich organ in the body (Orth, Bellosta, 2012). However, the occurrence of cancer can alter the expression and function of LRP1 (Shruthi et al., 2022, Xing et al., 2016). Studies have shown that LRP1 is upregulated in GBM cells in comparison to normal brain tissue meaning it may facilitate the uptake of growth factors, which promote tumour growth and invasion (Shruthi et al., 2022, Xing et al., 2016). Additionally, cholesterol is important for the growth and survival of glioma cells, which indicates the significance of LRP1 in GBM's pathophysiology (Shruthi et al., 2022, Guo, X. et al., 2022). Altogether, LRP1 plays a dual role since it maintains the integrity of the BBB and has impact on the pathological progression of GBM, making it a critical target in GBM (Shruthi et al., 2022, Guo, X. et al., 2022).

1.3 Blood-Brain Tumour Barrier

Various neurological diseases can impact the function and integrity of the BBB. Conditions including stroke, multiple sclerosis, epilepsy and brain tumours are associated with disruptions in the BBB, leading to an increased permeability and subsequently invasion of toxic substances into the BBB (van Tellingen et al., 2015). In the presence of brain tumours, especially GBM, the BBB undergoes significant alterations, which results in the formation of the blood-brain tumour barrier (BBTB) (van Tellingen et al., 2015).

1.3.1 Alterations in Vasculature

The BBTB is characterised by various morphological alterations, including increased angiogenesis, reduction of TJ expression, fewer mitochondria, shrinkage of astrocytic end-feet and thicker basal membranes (*see figure 4*) (Rathi et al., 2022, Machein et al., 1999). However, the alterations may vary depending on tumour type, grade, size and location (Belykh et al., 2020). It may also vary within the same tumour due to its heterogeneity (Belykh et al., 2020). The hypoxic environment in malignant gliomas increases pro-angiogenic factors leading to the development of new blood vessels that are leakier compared to BBB (Machein et al., 1999, Rathi et al., 2022). In addition, GBM cells also interact with already existing normal capillaries in the brain (Toyoda et al., 2013). These processes are a necessity for the tumour cells as the nutritional demand is increased (Arvanitis, Ferraro & Jain, 2020). The formation of these new vessels results in the decrease of TJ expression, especially claudin-5 and ZO-1 (Nitta et al., 2003). Based on a study, brain tumours have three different types of endothelia, including discontinuous, continuous fenestrated and non-fenestrated continuous capillaries, in which the last mentioned is similar to normal BCECs (Schlageter et al., 1999). In the non-fenestrated continuous capillaries, drug entry to the tumours would mostly occur through passive diffusion, whereas in continuous fenestrated, there is an increase in permeability for small substances and selective larger substances (Schlageter et al., 1999). Lastly, discontinuous capillaries have a further increased permeability to water-soluble compounds (Schlageter et al., 1999).

Depending on which grade glioma, the BBTB shows different structure and functions. In low-grade gliomas (I and II), the BBTB is mostly comparable to the normal BBB with slight upregulation of VEGF (Machein et al., 1999). Compared to low-grade gliomas, grade III gliomas have larger vessel size, vascular diameter and microvascular area (Guo, H. et al., 2019). In GBM, the alterations of the BBB are significant due to GBM's

infiltrating nature, which relocates astrocytic end-feet and decrease TJs in BCECs leading to the disruption of BBB integrity (Arvanitis, Ferraro & Jain, 2020, Belykh et al., 2020). The leakiness in BBTB causes various substances to enter the brain parenchyma, which increases the intracranial fluid pressure (Boucher, Y. et al., 1997). The increased fenestration in BBTB is a major factor in the formation of oedemas in GBM (Arvanitis, Ferraro & Jain, 2020, Boucher, Y. et al., 1997, Machein et al., 1999).

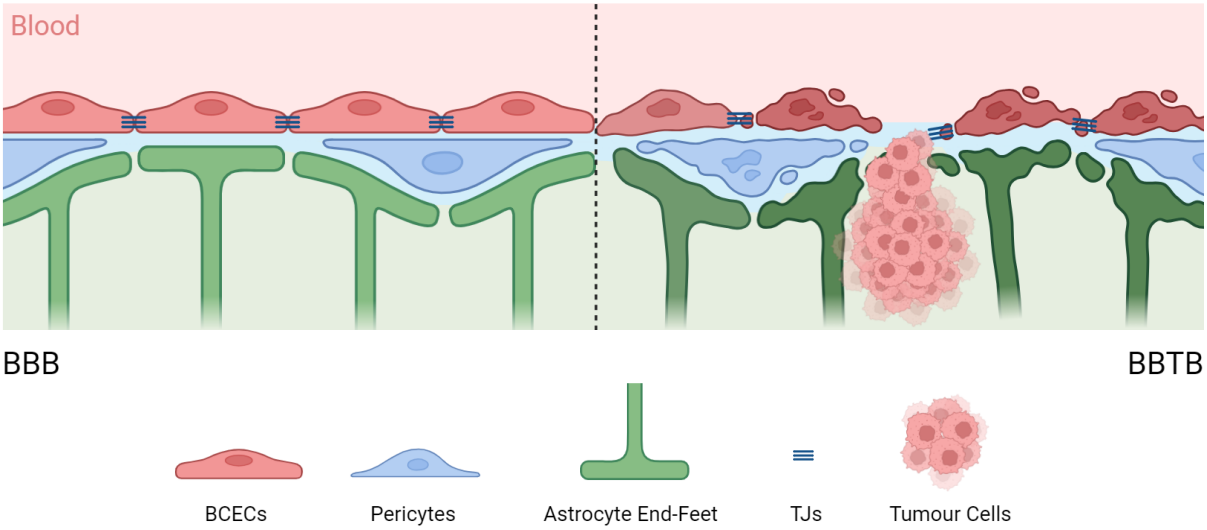

Figure 4: An overview of the blood-brain barrier (BBB) and blood-brain tumour barrier (BBTB). On the left, an intact BBB can be seen containing BCECs, pericytes, astrocytic end-feet and tight junctions. On the right, BBTB can be observed, in which the tumour cells cause disruption amongst the BCECs, pericytes, unattached astrocytic end-feet and downregulation of tight junctions. BCECs: brain capillary endothelial cells, TJs: tight junctions. Inspired by (Profaci et al., 2020, Arvanitis, Ferraro & Jain, 2020, Belykh et al., 2020). Created in BioRender.com.

Despite the changes in BBTB, it has been observed that not the entire BBB is affected by GBM (Arvanitis, Ferraro & Jain, 2020). However, an *in vivo* study by Toyoda observed that GBM cells influence the BBB by secretion of fibroblast growth factor 2 (FGF-2), which significantly increased the expression of ZO-1 and occluding, indicating that FGF-2 improved the endothelial function of the BCECs (Toyoda et al., 2013). FGF-2, also known as basic fibroblast growth factor (bFGF), is an oncogenic factor in GBM, which plays a role in growth and vascularisation of gliomas (Jimenez-Pascual et al., 2020). All in all, angiogenesis is an important factor to consider in the treatment or delivery of pharmacotherapeutic drugs of GBM.

2. Aim

The main purpose of this thesis was to explore the correlations between GBM associated cell types, T10 and U87, and the disruption of BBB, which led to the following research question:

Do the glioblastoma multiforme associated cell types, T10 and U87, induce alterations in the blood-brain barrier, resulting in a decline in its integrity?

Additionally, this thesis consisted of subsidiary aims, which contributed to the main aim, being the following:

1. Isolate PBECs to use for constructing a functioning BBB/BBTB model
2. Investigate the effect of T10 and U87 cells on BBB models using TEER
3. Staining of the BBB/BBTB models after termination to visualise the expression of the TJ protein claudin-5
4. Investigate the genetic expression of biomarkers in BBB models, including claudin-5, ZO-1, TfR1, VEGFR1, P-gp and LRP1
5. Investigate the genetic expression of biomarkers in T10 and U87 cells that can alter the BBB, including EGFR, VEGF-A, COX-2 and Ang-2
6. Examine T10 in *in vivo* murine models via immunohistochemistry (IHC)

3. Materials and Methods

3.1 Cultivation of T10 and U87

Prior to cultivation of the GBM associated cells, a cancer medium was prepared containing Neurobasal™-A Medium (#10888-022, Gibco), 1% penicillin/streptomycin (x100) (#15140-122, Gibco), 1% Glutamin-L 200 mM, 1% B27 supplement without vitamin A (50X) (#12587-010, Gibco), 0.5% N2 supplement solution (x100) (#17502-048, Gibco) and 25 ng/mL Epidermal Growth Factor (#E9644, Sigma Aldrich), which was sterile filtered into a blue cap bottle and stored at 4°C for maximum of two weeks. For every passaging or medium renewal with the cancer medium, 25 ng/mL of bFGF (#100-18B, PreproTech) was freshly added.

Two vials, one with T10 and another with U87, were taken from the cryotank and thawed using warm water for around 1-2 minutes, which then was followed by a centrifugation step with cancer medium at room temperature for 5 minutes at 1200 rpm. The supernatant was removed followed by the cells being resuspended in cancer medium. Afterwards, the cells were seeded into two respective T25 flasks and incubated at 37°C with 5% CO_2. When the cells would become confluent, medium renewal would take place, which was approximately around 1-2 times per week. The cancer medium with cells from the T25 flasks would be centrifuged at room temperature for 5 minutes at 1000 rpm and then transferred back to their respective flasks with new cancer medium and incubated at 37°C with 5% CO_2. The GBM cell lines were cultured for at least two weeks prior to use in any experiments.

3.1.1 T10 and U87

T10 is a newer human GBM cell line, which were obtained from a patient in 2019 at Rigshospitalet, Denmark. In this thesis, T10 was obtainable due to the collaboration with Kræftens Bekæmpelse. This cell line has been through fewer passages, indicating that T10 still preserves various of the original characteristics (Boccellato, Rehm, 2022).

U87 is a widely known human GBM cell line, which was obtained from a 44-year-old female patient in 1966 at Uppsala University, Sweden (Boccellato, Rehm, 2022, Allen et al., 2016, Dolgin, 2016). This cell line is commonly used in GBM research, resulting in the many passages of the cells and it is considered an immortalised cell line (Boccellato, Rehm, 2022). Due to cancer's heterogeneity, the cells have different genetic characteristics from passage to passage (Boccellato, Rehm, 2022).

Both of the above-mentioned human GBM cell lines have been used to investigate the different elements in this thesis.

3.2 Blood-Brain Barrier and Blood-Brain Tumour Barrier Models

3.2.1 Isolation of Porcine Brain Capillary Endothelial Cells

The protocol in this thesis used for the isolation of porcine BCECs (PBCECs) is made by Thomsen et. al. (Thomsen, L. B., Burkhart & Moos, 2015)

Around 12-14 domestic half pig brains were obtained from Danish Crown, Denmark, and had a transportation time of 2 hours before arriving at Aalborg University. Firstly, the meninges were removed following the collection of 10-12 g of cortex in petri dishes containing ice-cold Dulbecco's Modified Eagle Medium (DMEM/F12) medium (#31331-028, Gibco). The tissue was cut into small pieces and then transferred into a 50 mL tube, which contained DMEM/F12 with 1 mg/mL collagenase type II (#17101105, Gibco) and 20 µL/mL DNase I (#D4513, Sigma Aldrich), resulting in the degradation of the tissue. The homogenate was incubated at 37°C for 1 hour and 15 minutes at 200 rpm in an incubating mini shaker (VWR). Subsequently, DMEM/F12 was added to the suspension followed by a centrifugation step at 4°C for 8 minutes at 1000 g in order to stop the degradation of the tissue. The supernatant was aspirated, and the cells were resuspended and centrifuged in DMEM/F12 including 20% bovine serum albumin (BSA) (#EQBAH62, Europa Bioproduct) at 4°C for 20 minutes at 1000 g. After centrifugation, the myelin layer including neurons and glial cells was discarded. The cell pellet containing the microvessels was transferred to a new 50 mL tube with DMEM/F12 containing 1 mg/mL collagenase-dispase (#11097113001, Sigma Aldrich) and 7.5 µg/mL DNase I and centrifuged at 37°C for 50 minutes at 200 rpm in order to degrade extracellular constituents. DMEM/F12 was added to the cell pellet and centrifuged at 4°C for 5 minutes at 700 g. The microvessels were separated by centrifugation at 4°C for 10 minutes at 1000 g in a percoll (#P1644, Sigma Aldrich) gradient containing 61% phosphate-buffered saline (PBS), 3% 10X PBS (14200-067, Gibco) and 3% fetal calf serum (FCS), which was sterile filtered and centrifuged at 4°C for 65 minutes at 21000 rpm prior use for this step. A syringe was utilised to collect the microvessels and transferred to a new 50 mL tube containing DMEM/F12, which was centrifuged at 4°C for 10 minutes at 1000 g. Next, the supernatant was removed and the microvessels were resuspended in DMEM/F12 followed by a centrifugation step at 4°C for 7 minutes at 700 g to remove percoll residues.

The microvessel pellet was resuspended in a PBCEC medium containing DMEM/F12, 10% plasma derived bovine serum (PDS) (First Link Ldt, UK), 1 mg/mL insulin-transferrin-selenium (ITS) (#11074547001, Roche), 50 mg/mL gentamicin (#17-518Z, Lonsa) and 1 ng/mL bFGF (#1363-697, Roche). Lastly, 4 µg/mL puromycin (#P8833/P7255, Sigma Aldrich) and 15 µg/mL chloramphenicol (AAU, Denmark) was added.

The cell suspension was plated in pre-coated culture dishes with a coating containing sterile miliQ (AAU, Denmark) with 0.05 mg/mL fibronectin (#F1141, Sigma Aldrich) and 0.15 mg/mL collagen IV (#C5533, Sigma Aldrich) followed by an incubation period of 2 days at 37°C and 5% CO_2 for the PBCECs to sprout from the microvessel fragments. Upon reaching a cell confluency of approximately 70-80%, the PBCECs were either used directly for *in vitro* BBB and BBTB models or frozen in PBCEC medium with 30% FCS and 7.5% DMSO at -70°C.

3.2.2 Porcine Blood-Brain Barrier Models

The isolated PBCECs were used to generate a BBB model. Filter inserts (#665610, Greiner Bio-One) were prepared with a coating containing sterile miliQ with 0.5 mg/mL collagen IV and 0.1 mg/mL fibronectin, which were placed in 12-well plates and incubated at 37° with 5% CO_2 for 60 minutes prior use. These 1.13 cm^2 filters inserts with 1 µm pore diameters were then seeded with approximately 100,000 PBCECs in each. Additionally, 1.5 mL of PBCEC medium was added to the wells whereas 0.5 mL was added to the filters followed by an incubation period of 24 hours at 37°C with 5% CO_2 before the measurement of TEER.

3.2.2.1 Trans-Endothelial Electrical Resistance

For the investigation of the BBB and BBTB models' integrity, TEER was measured daily using a Millicell ERS-2 Epithelial Volt-Ohm Meter (#MERS00002, Millipore) with Millicell ERS-Electrodes (#MERSSTX01, Millipore) attached to it. For each filter, TEER would be measured three times from which the average would be calculated from. To determine the TEER values, the mean TEER from a control filter with only PBCECs medium was subtracted from the mean TEER values from each of the filters in the BBB and BBTB models. Lastly, the difference in the TEER values was multiplied by the area of the filter being 1.13 cm^2. All TEER value results were presented as $\Omega \cdot cm^2$.

3.2.2.2 Induction of Porcine Blood-Brain Barrier

Upon reaching confluency along with TEER values of 30 to 60 $\Omega \cdot cm^2$, the PBCECs have formed a uniform layer ready to be induced for TJ formation. This thesis consisted of 3 different barrier models (*see figure 5*): monoculture with PBCECs, co-culture with PBCECs and T10, and co-culture with PBCECs and U87. The medium in the filters for all three barrier models was replaced with PBCEC medium supplemented with 550 nM hydrocortisone (#H4001, Sigma Aldrich), 250 µM pCPT-cAMP (#C3912, Sigma Aldrich) and 17.5 µM RO-20-1724 (#B8279, Sigma Aldrich). The wells for the monoculture were replaced with PBCEC medium supplemented with 550 nM hydrocortisone. For both co-cultures, the wells were prepared with the respective GBM cell lines with a density of 30,000 cells pr. cm^2 and a 1:1 mix of cancer medium and PBCEC medium supplemented with 550 nM hydrocortisone.

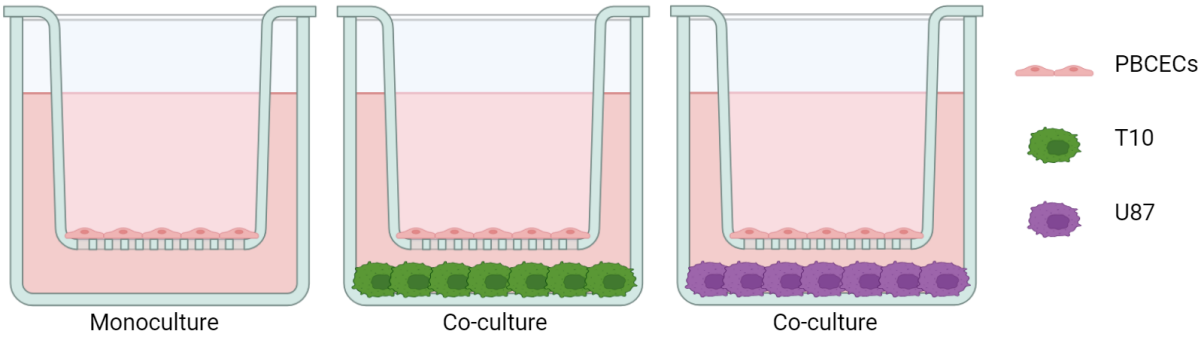

Figure 5: An overview of the three barrier models. From left to right, the first model is a monoculture including only PBCECs, the second model is a co-culture with PBCECs and T10 cells and the third model is a co-culture with PBCECs with U87 cells. PBCECs: porcine brain capillary endothelial cells. Created in BioRender.com.

3.2.3 Immunocytochemistry of Barrier Models

The cells were gently washed in each filter with PBS twice followed by a fixation with 4% paraformaldehyde for approximately 5-10 minutes. Then the cells were washed again with PBS twice to remove the remaining residue of paraformaldehyde.

A blocking buffer containing 3% BSA and 0.3% Triton X-100 in KPBS was prepared. Every mentioned incubation or washing step in the following below was done on The Belly Dancer (Stovall Life Science, Inc.) at 44 rpm. For each filter and well, blocking buffer was added. This blocking process lasted 60 minutes at room temperature. Afterwards, the blocking buffer was removed from the filters, and the cells were incubated with polyclonal rabbit anti-claudin-5 (#SAB4502981, Sigma Aldrich) diluted in 1:300 in blocking buffer for one hour at room temperature. This was followed by three washing steps of each 5 minutes using washing buffer, which is blocking buffer diluted 1:50 in KPBS.

Simultaneously, the blocking buffer in the wells was replaced with washing buffer. Alexa Fluor 488 goat anti-rabbit (#A11034, Invitrogen) diluted 1:500 in blocking buffer was added and incubated for one hour at room temperature whilst covered in tin foil since it is light sensitive. The cells were washed once with PBS for 5 minutes in both the filters and the wells. Lastly, cellular staining was done using DAPI, which was diluted 1:500 in KPBS and incubated for 5 minutes at room temperature. This was followed by two washing steps of PBS for 5 minutes. The filters were mounted on object slides using DAKO fluorescent mounting media (Agilent Technologies, Inc.) where the cells were facing the cover slips.

3.2.4 *In Vitro* Gene Expression

3.2.4.1 RNA Purification

The RNA purification was done using Thermo Scientific GeneJET RNA Purification Kit (#K0732, Thermo Scientific). For the RNA purification of T10 and U87 cells, the supplied protocol by the manufacturer was followed. Prior to the RNA purification in the BBB and BBTB models, the PBCECs medium was removed from the filters followed by two washing steps with PBS to remove residual medium.

For the BBB and BBTB models the following described was done. Lysis buffer containing 14.3 M β-mercaptoethanol was prepared where 400 µL of lysis buffer mixture was added to pool three filters together from the barrier models, which was transferred to a RNase-free microcentrifuge follow by vortex for 10 seconds. Afterwards, 240 µL of 96% ethanol was added and mixed thoroughly by pipetting. The lysate with ethanol was transferred to the GeneJET RNA Purification Columns and centrifuged at 4°C for 1 minute at ≥12000 g. The flow-through solution was discarded and replaced with a new 2 mL collection tube. Subsequently, 700 µL of Wash Buffer 1 was added and then centrifuged at 4°C for 1 minute at ≥12000 g. The flow-through was discarded, 600 µL of Wash Buffer 2 was added and centrifuged at 4°C for 1 minute at ≥12000 g. Again, the flow-through was discarded and a last washing step with 250 µL of Wash Buffer 2 was added followed by centrifugation at 4°C for 2 minutes at ≥12000 g. After removing the flow-through, the GeneJET RNA Purification Columns were transferred to a sterile 1.5 mL RNase-free microcentrifuge tube followed by 25 µL of nuclease free water being added to the centre of the column, which was centrifuged at 4°C for 1 minute at ≥12000 g to elute the RNA. The last step with the 25 µL of nuclease free water was repeated to maximise the RNA yield, resulting in a total volume of 50 µL with RNA.

3.2.4.2 DNase Treatment and cDNA Synthesis

The RNA samples were treated with DNase I, RNase-free (#MAN0012000, Thermo Scientific) to ensure the degradation of residual DNA. This was followed by a cDNA synthesis done using Thermo Scientific Maxima H Minus First Strand cDNA Synthesis Kit (#K1651, Thermo Scientific). Both kits were done following the manufacturer's protocols.

3.2.4.3 RT-qPCR

The primers used for the reverse transcription-quantitative polymerase chain reaction (RT-qPCR) was either found in articles related to thesis (Roelofs et al., 2014, Koga et al., 2001) or designed in Primer-BLAST in the National Center for Biotechnology Information database and then ordered from Tag Copenhagen A/S. The sequences of the homo sapiens' primers used for RT-qPCR analysis of T10 and U87 can be seen in table 2, whereas the sus scrofa ones for the analysis of BBB and BBTB models can be seen in table 3. Actin and HPRT1 were used as housekeeping genes.

Table 2: Homo sapiens primer sequences used for the RT-qPCR analysis of T10 and U87 cells. Forward and reverse primer sequences for housekeeping genes (actin and HPRT1) and genes of interest (EGFR, VEGF-A, COX-2 and Ang-2) with each their respective reference sequences.

Target	Forward	Reverse	Ref. Sequence
Actin	CCGCCGCCAGCTCACCAT	GCCCCACGATGGAGGGAAAG	NM_001101.5
HPRT1	GCCCTGGCGTCGTGATTAGT	TGGCCTCCCATCTCCTTCATCA	NM_000194.3
EGFR	CTGGGGTGCAGGAGAGGAGA	TCGGAATTTGCGGCAGACCA	NM_201283.2
VEGF-A	ATAAGTCCTGGAGCGTGTACGTTG	TTGCAGGAACATTTACACGTCTGC	NM_001025366.3
COX-2	CCGGGTACAATCGCACTTAT	GGCGCTCAGCCATACAG	NM_000963.4
Ang-2	GGATCTGGGGAGAGAGGAAC	CTCTGCACCGAGTCATCGTA	NM_001386337.1

Table 3: Sus scrofa primer sequences used for the RT-qPCR analysis of the BBB and BBTB models. Forward and reverse primer sequences for housekeeping genes (actin and HPRT1) and genes of interest (claudin-5, ZO-1, VEGFR1, TfR 1, P-gp and LRP1) with each their respective reference sequences.

Target	Forward	Reverse	Ref. Sequence
Actin	CAGAGCGCAAGTACTCCGTGTGGAT	GCAACTAACAGTCCGCCTAGAAGCA	XM_003124280.2
HPRT1	AATGCAAACCTTGCTTTCCTTGGTC	GGCATAGCCTACCACAAACTTGTCT	NM_001032376.2
Claudin-5	GTCTTGTCTCCAGCCATGGGTTC	GTCACGATGTTGTGGTCCAGGAAG	NM_001161636.1
ZO-1	AAGCCTCCAGAGGGAGCATCTAA	ATATCTTCAGGTGGCTTCACTTGGG	XM_021098896.1
VEGFR1	CACCCCGGAAATCTATCAGATC	GAGTACGTGAAGCCGCTGTTG	XM_021065524.1
TfR 1	TTGATGATGCTGCTTTCCCTTTCCT	CCATTCTGTTCAACTGAGGAACCCT	NM_214001.1
P-gp	CGATGGATCTTGAAGAAGGCCGAAT	CCAGTTTGAATAGCGAAACATGGCA	XM_003130205.2
LRP1	CAATAGCGACGAGGCTGGCT	TGGTGCAGTTGGCGTGTGTT	XM_021091826.1

The efficiency of the primers for EGFR, VEGF-A, COX-2 Ang-2, VEGFR1 and LRP1 were tested by creating standard curves using a tenfold dilution of cDNA (10x, 1x, 0.1x, 0.01x and 0.001x). The remaining primers' efficiencies were validated prior to this thesis. To ensure that only one product was amplified, the melt curves were examined. Primer efficiencies between 92% and 108% and calculated correlation coefficients $R^2 > 0.95$ were accepted.

All the samples for the RT-qPCR were analysed in triplicates for each gene (*see table 2 and 3*) in 96-well plates (#4ti-0761, Azenta Life Sciences). For each reaction, 2 ng cDNA was mixed with 5 µL Maxima SYBR Green qPCR Master Mix with 0.02 µM ROX (#K0252, Thermo Scientific), 0.03 µL forward primer (100 pmol/µL) and 0.03 µL reverse primer (100 pmol/µL). A reverse transcriptase (RT-) control was included for every RNA sample in order to detect any possible genomic DNA contamination. Moreover, a no template control (NTC) was added for each gene to detect any potential contamination of the PCR reagents and to ensure that the amplification observed is from the target DNA. All RT-qPCR plates were run on the QuantStudio 6 Flex Real-Time PCR System (Thermo Scientific) with the following thermal settings: 95°C for 10 minutes, 40x cycles at 95°C for 15 seconds and at 60°C for 1 minute, which lastly was followed by the melting curve formation to verify the amplified product and had the following thermal settings: 95°C for 15 seconds, 60°C for 1 minute and 95°C for 15 seconds.

For the experiments with the GBM associated cells, the data was presented as relative gene expression (RGE) compared to the U87 cell line whereas for the BBB and BBTB experiments, the data was presented as RGE compared to the monoculture with only PBCECs.

3.3 *In Vivo* Xenograft Mouse Model

3.3.1 Xenotransplantation of T10

The xenotransplantation of T10 in the mice used in this thesis was performed by the supervisor. Six-week-old nude mice weighing around 20-30 g were anesthetised and placed on a stereotactic frame where a cranial incision was made to expose bregma. A hole was drilled 1.5 mm lateral, 1 mm anterior and 3 mm deep into the bregma at the left side where the injection with 300,000 T10 cells in 10 µL cancer medium was placed and slowly injected into the brain parenchyma over a period of 5 minutes. Once the injection was done, the needle was left inside for 3 minutes before removal to prevent cells from exiting the burr hole and then removed gently. The burr hole was covered with bone wax and the skin was stitched up. The mice were transferred to a heated cage till they were recovered and were euthanised 3 weeks after the operation.

3.3.2 Storage of Brains

After surgical removal of the mouse brains, it was transferred to a small container with KPBS containing 1% sodium azide to prevent contamination. Prior sectioning of the brains, they were transferred to a different solution consisting of 70% KPBS and 30%

sucrose. The brains were in this solution for four days to drain them from remaining water as a prevention of crystallisation when frozen.

3.3.3 Cryo-sectioning

Leica CM3050 S Research Cryostat was utilised to section the brains and had the following settings: CT -23°C, OT -22°C, slice sectioning at 40 µm with a knife angle at 7°. For mounting of the brains, Tissue-Tek® O.C.T. Compound (Sakura Finetek) was used. After mounting them onto the specimen chucks, the brains were further completely covered in Tissue-Tek. The sectioned samples were transferred to small containers with KBPS. This was followed by a washing step with antifreeze, which contained 35% ethylene glycol (Sigma Aldrich), 35% sucrose, 29% 0.2M phosphate buffer and 1% PVP-40 (Sigma Aldrich). Lastly, all the samples were transferred into cryotubes containing antifreeze and stored at -20°C.

3.3.4 Immunohistochemistry of T10

The immunohistochemistry (IHC) of T10 was a three-day experiment, which will be explained in the following section. The biomarkers investigated in *in vivo* in this thesis include claudin-5, VEGFR1 and P-gp (*see table 4*). In addition, their respective primary and secondary antibodies and the staining methods can be seen in table 4.

Table 4: An overview of the primary and secondary antibodies for claudin-5, VEGFR1 and P-gp. The table shows the corresponding primary and secondary antibodies for each of the biomarkers, and it includes the dilutions for each of the antibodies, catalogue numbers and manufacturer and lastly, the staining methods.

Biomarker	Primary antibody	Secondary antibody	Staining
Claudin-5	Rabbit Claudin-5 1:200 in blocking buffer #SAB450298, Sigma Aldrich	Anti-rabbit (goat) 1:500 in washing buffer #BA-1000, Vector Laboratories Inc.	ABC DAB
VEGFR1	VEGFR1 PaB to Vascular Endothelial (rabbit) 1:200 in blocking buffer #MBS2027946, Mybiosource	Anti-rabbit (goat) 1:500 in washing buffer #BA-1000, Vector Laboratories Inc.	ABC DAB
P-gp	Anti PGP/MDR-1 mouse 1:200 in Solution B #MA1-26530, Pierce	Anti-mouse (rabbit) 1:500 in Solution B #E0354, DAKO	M.O.M ABC DAB

During all the incubation and washing steps, the samples were placed on The Belly Dancer at 44 rpm, excluding the steps in the fume hood. Three cryotubes with brains sections were transferred to three different small containers and washed in KPBS three times for 5 minutes. Afterwards, the brain sections that would be stained with claudin-5 and VEGFR1 were incubated in a blocking buffer containing KPBS with 3% BSA and 0.3% Triton X-100 at room temperature for 60 minutes. The M.O.M kit was used for P-gp staining to

block unspecific binding, since the primary antibody was obtained from mice. The brain sections for P-gp staining were incubated in M.O.M solution A (*see table 5*) at room temperature for 60 minutes, which were followed by two washing steps with KPBS for 5 minutes. Subsequently, the brain sections for P-gp staining were incubated with M.O.M. solution B at room temperature for 5 minutes (*see table 5*). Lastly, all samples were incubated with their corresponding primary antibodies (*see table 4*) at 4°C overnight.

Table 5: An overview of the different solutions applied in the immunohistochemistry. This table incudes the names of the different solutions including the components applied with their respective catalogue numbers and manufacturer.

Solution	Components	Cat. Nr.
M.O.M. Solution A	5 mL KPBS 4 drops stock solution Mouse Ig 22 µL Triton X-100	- #BMK-2202, Vector Laboratories, Inc. #X100, Sigma Aldrich
M.O.M. Solution B	7.5 mL KPBS 600 µL Protein concentration	- #BMK-2202, Vector Laboratories, Inc.
ABComplex Vectastain	3 drop solution A 3 drop solution B 15 mL KPBS	#PK-6100, Vector Laboratories, Inc. #PK-6100, Vector Laboratories, Inc. -
DAB	2 mL DAB 18 mL 0.05M Tris/HCl pH = 7.6 6.6 µL H2O2 immediately before use	#D5637, Sigma-Aldrich - #H1009, Sigma-Aldrich

On the second day, the claudin-5 and VEGFR1 samples were washed three times with washing buffer for 5 minutes, which is the blocking buffer diluted 1:50 in KPBS, whereas the P-gp samples were washed three times in KPBS for 5 minutes. For all samples, this was followed by an incubation step of the corresponding secondary antibodies (*see table 4*) at room temperature for 60 minutes. Afterwards, the claudin-5 and VEGFR1 samples were washed three times in washing buffer for 5 minutes and the P-gp samples were washed in KPBS for 5 minutes. This was followed by an incubation step with Vectastain solution for all samples at room temperature for 30 minutes, however, the Vectastain solution was prepared 30 minutes prior to use. The samples were washed twice with KPBS for 5 minutes followed by a washing step with 0.05M Tris/HCl for 5 minutes. Under the fume hood, 0.05M Tris/HCl was replaced with DAB solution where the samples were incubated at room temperature for 10 minutes while stirred. Subsequently, 0.05M Tris/HCl was added to the samples and incubated at room temperature for 5 minutes in the fume hood, which was followed by two washing steps with KPBS at room temperature for 5 minutes. Lastly, the brain sections were transferred to a petri dish with 0.5% gelatine and collected onto object glasses left drying overnight.

On the third day, the object glasses were sealed using Pertex Mouting Medium (Histolab) on a coverslip and were left to entirely dry in the fume hood prior to microscopy.

3.4 Microscopy

The immunocytochemistry (ICC) samples were examined and imaged with a Zeiss Axioplan 2 (Carl Zeiss A/S) non-inverted microscope including AxioCam MRc (Carl Zeiss A/S) and Zeiss ZEN version 3.4 whereas the IHC samples were examined and imaged with a Leica DM5500 B including JenOptik Gryphax. The images were processed in Fiji ImageJ version 1.54 (Fiji Software) and arranged in InkScape. The images in section 4.5 for claudin-5 were taken from my previous 7th semester project.

3.5 Statistical Analysis

The statistical analyses were performed in GraphPad Prism version 10.3.0 (GraphPad Software, USA). All data would be investigated for normal distribution using Shapiro-Wilk with following condition $p < 0.05$. When two groups were compared, depending on normal distribution or not, either an unpaired t-test or Mann-Whitney test was utilised, respectively. For multiple group comparisons, depending on normal distribution, either a one-way ANOVA or Kruskal-Wallis test was performed, correspondingly. When $p < 0.05$, the results were considered as statistically significant. All data is presented as mean ± SEM.

4. Results

4.1 TEER of PBCECs in BBB and BBTB Models

4.1.1 Pilot Experiment with BBB and BBTB Model

Prior to the main experiments, a pilot experiment was conducted to preliminarily assess the effect of T10 on the BBB and thereby investigate the integrity of the BBB. This pilot experiment consisted of a monoculture with PBCECs, which will be referred to as control in this entire result section, and a co-culture with PBCECs and T10 cells, which were cultivated for 3 weeks prior to use in this experiment. TEER was measured every 24 hours over a period of 20 days to determine changes in the two barriers' integrity. Both of these barrier models generated TEER values of 72 ± 7.81 before the induction of the barrier at day 0. At day 1, the barriers were induced, which was determined by the increase in their TEER values, which was 292 ± 29.5 for the monoculture and 406 ± 147.7 for the co-culture. Figure 6 illustrates the TEER measurements over 20 days, which creates a time-lapse model over this experimental pilot set-up. The TEER values for both barrier models were progressively increasing up until day 5 whereafter they were slowly declining. On day 8, new medium was added for each of the barrier models in both the filters and wells. This was followed by an increase in the TEER values in the co-culture with T10, whereas the control continued declining progressively. An unpaired t-test was performed over the entirety of the pilot experiment for the two groups, which indicated a significant increase in TEER values for the co-culture with T10 compared to the control ($p < 0.0001$).

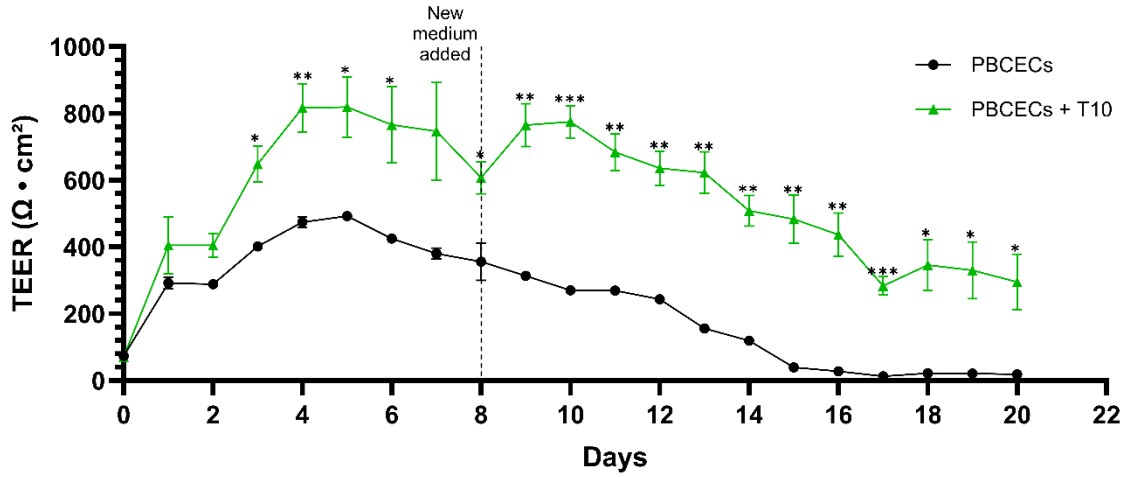

Figure 6: TEER measurements of the pilot experiment. The figure presents TEER measurements over 20 days for the control (black with dot) and co-culture with T10 cells (green with triangle). The dotted line indicates when new medium was added to the barrier models, which was on day 8. The co-culture with T10 ($n = 3$) was significantly higher than the control ($n = 3$) on day 3-6 and 8-20 ($***,\ p < 0.001$). n equals the number of filter inserts, and all values are presented as mean TEER ± SEM.

4.1.2 BBB and BBTB at End

Two follow-up experiments were conducted to investigate the effect of the GBM associated cell lines on the BBB's integrity, which will be referred to as experiment 1 and 2. These experiments consisted of three set-ups, including monoculture with only PBCECs and two co-culture groups with GBM associated cell lines, T10 and U87. Similarly to the pilot experiment, TEER was measured every 24 hours.

Prior to the induction in experiment 1 at day 0, the barrier models generated TEER values of 52 ± 13.7, whereas at day 1, the TEER values were increased to 334 ± 123 for the control, 584 ± 131.4 for the co-culture with T10 cells and 572 ± 112.4 for the co-culture with U87 cells. For experiment 1, the GBM cells were cultivated for 3 weeks prior to use and new medium was added on day 7, 13 and 18. Figure 7a presents the TEER measurements over 21 days, which shows the increase of TEER values in the control till day 7 whereafter it progressively declines till the end. Both co-cultures were increasing in TEER values till day 2 whereafter they were declining till day 7 followed by a progressive increase till day 13 and slowly declining till the end of the barrier models. ANOVA was performed and revealed a significant different between the groups ($p = 0.0003$). Further unpaired t-tests were performed between the control and each of the co-cultures, which showed that there was a significant difference between the control and co-culture with T10 ($p = 0.0016$) but no significant difference between the control and co-culture with U87.

In experiment 2, which lasted 13 days, the set-up from experiment 1 was replicated, however, the GBM cells were cultivated for 10 weeks. On day 0, the barrier models generated TEER values of 72 ± 7.4 whereas on day 1, the TEER values increased to 187 ± 14.9 for the control, 319 ± 15.7 for the co-culture with T10 and 177 ± 55.9 for the co-culture with U87. New medium was added on day 7 and 11 for all three barrier models. All barrier models were increasing in TEER values till day 5 followed by a slow decline till day 7 (*see figure 7b*). From day 7, the control progressively kept declining till the end of the experiment whereas the co-culture with U87 was steady until the end. The co-culture with T10 had a peak increase on day 8 followed by a drop on day 9 and slow increase till day 12. Kruskal-Wallis was performed and showed a significant difference between the groups ($p < 0.0001$). Additionally, Mann-Whitney U tests were performed, which showed only a significant difference between the control and co-culture with T10 ($p < 0.0001$).

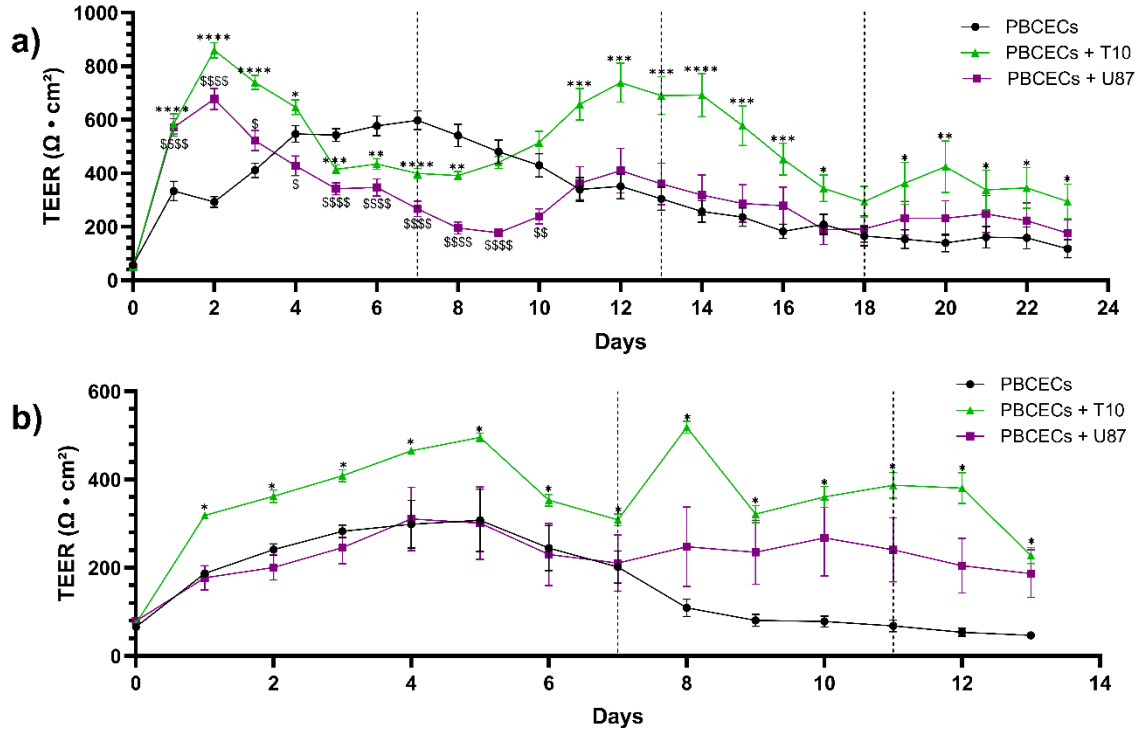

Figure 7: TEER measurements over experiment 1 and 2 till the end. Figure a depicts the illustration of the control ($n = 12$), co-culture with T10 ($n = 12$) and co-culture with U87 ($n = 12$). The TEER values were measured over 23 days and new medium was added on day 7, 13 and 18, which is indicated by the dotted lines. Additionally, the TEER values were significantly higher for the co-culture with T10 compared to the control for all days except day 9 and 10 ($****$, $p < 0.0001$). The TEER values of the co-culture with U87 are significantly higher than the control on day 1, 2 and 3 whereafter they are significantly lower from day 4 to 10 ($\$\$\$$, $p < 0.0001$). Figure b depicts the three barrier models: control ($n = 4$), co-culture with T10 ($n = 4$) and co-culture with U87 ($n = 4$). They were measured over 13 days and new medium was added on day 7 and 11 (dotted lines). Data indicates that the co-culture with T10 was significantly higher than the control throughout the entirety of the experiment ($*$, $p < 0.05$). * is used to show significant differences between the control and co-culture with T10 whereas $ is used to show significant differences between the control and co-culture with U87. The control is black with dots, co-culture with T10 is green with triangles and co-culture with U87 is purple with squares. n equals the number of filter inserts, and all values are presented as mean TEER ± SEM.

4.1.3 BBB and BBTB at Day 6 and End

Two additional experiments were conducted, which will be referred to as experiment 3 (ended on day 6 and end of experiment) and experiment 4 (ended on day 6 and end of experiment). Experiments 3 and 4 also consisted of three barrier models: control, co-culture with T10 and co-culture with U87. In these experiments, all three barrier models were set up to end on day 6 and at the end where the last mentioned is similar to pilot and experiment 1 and 2. Both of the experiments were divided into ending at day 6, which was to investigate the barrier function when the TEER values would be high, and at the end to investigate the barrier function when the TEER values would be lower.

Experiment 3 (for both end at day 6 and end of experiment) at day 0, the barrier models generated TEER values of 74 ± 10.6 whereas at day 1, the TEER values increased to 365 ± 35.9 in the control, 497 ± 21.8 in the co-culture with T10 and 439 ± 84.9 in the co-culture with U87. In experiment 3, the GBM cells were cultivated for 19 weeks prior to use, and new medium was added on day 6 and 10 of the experiment. Experiment 4 (for both end at day 6 and end of experiment) at day 0, the barrier models generated TEER values of 74 ± 6.3 whereas on day 1, the TEER values were increased to 320 ± 42.0 in the control, 466 ± 46.7 in the co-culture with T10 and 415 ± 32.2 in the co-culture with U87. In experiment 4, the GBM cells were cultivated for 23 weeks prior to use, and new medium was added on day 6 and 9 of the experiment. Figures 8a and 8c present the TEER measurements over 6 days, whereas figures 8b and 8d were measured over 14 days. In experiment 3 and 4, which ended on day 6, ANOVA tests were performed indicating no significant difference between the barrier models. For experiment 3, which ended at the end of the experiment, a Kruski-Wallis was performed indicating a significant difference between the three barrier models ($p < 0.0001$). Furthermore, Mann-Whitney U tests were performed between the control and each of the co-cultures, which showed a significant difference between the control and co-culture with T10 ($p = 0.0001$) and between the control and co-culture with U87 ($p = 0.0099$). Experiment 4 only showed a significant difference when a Mann-Whitney was performed between the control and co-culture with U87 ($p = 0.05$).

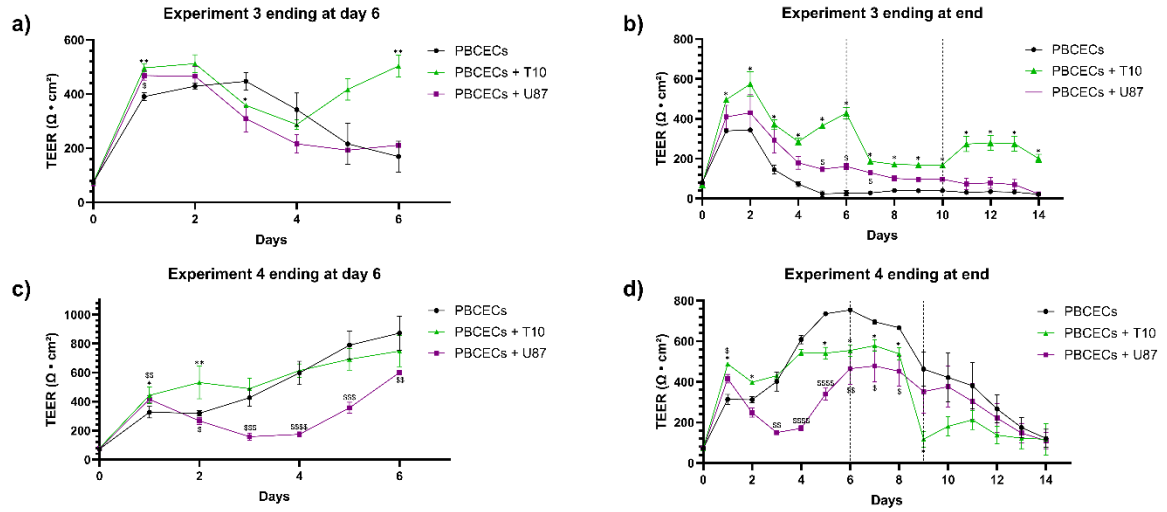

Figure 8: TEER measurements over experiment 3 and 4 ending at day 6 and at the end of the experiment. All graphs present the control (n = 4), co-culture with T10 (n = 4) and co-culture with U87 (n = 4). For figure a and c, the TEER values were measured over 6 days whereas figure b and d were measured over 14 days. On figure b, new medium was added on day 6 and 10, and on figure d, new medium was added on day 6 and 9. Figure a showed significant difference between the control and co-culture with T10 on day 1, 3 and 6 ($**, p < 0.01$) along with significant difference between the control and co-culture with U87 on day 1 ($\$, p < 0.05$) in experiment 3 ending at day 6. On figure b, the co-culture with T10 was significantly different from the control throughout the entirety of the experiment ($*, p < 0.05$), whereas there only was a significant difference between the control and co-culture with U87 from day 5 to 7 ($\$, p < 0.05$) in experiment 3 at the end of the experiment. Figure c showed significant difference between the control and co-culture with T10 on day 1 and 2 ($**, p < 0.01$), and a significant difference between the control and co-culture with U87 from day 1 till the end at day 6 ($\$\$\$, p < 0.0001$) in experiment 4 ending at day 6. Lastly, figure d showed a significant difference between the control and co-culture with T10 at day 1, 2, 5, 6, 7 and 8 ($*, p < 0.05$), and a significant difference between the control and co-culture with U87 at day 1 and from day 3 to 8 ($\$\$\$, p < 0.0001$) in experiment 4 at the end of the experiment. * is used to show significant differences between the control and co-culture with T10 whereas $ is used to show significant differences between the control and co-culture with U87. The control is black with dots, co-culture with T10 is green with triangles and co-culture with U87 is purple with squares. n equals the number of filter inserts, and all values are presented as mean TEER ± SEM.

4.2 Gene Expression of BBB and BBTB Models

RNA from PBCECs was isolated from each of the three barrier model set-ups: monoculture, co-culture with T10 and co-culture with U87. This was done for each set-up by pooling three of their corresponding filter inserts with PBCECs together forming an RNA sample ($n = 1$). The purpose of this was to investigate the RGE of the following biomarkers, including claudin-5, ZO-1, TfR, VEGFR1, P-gp and LRP1. Furthermore, the expression of the housekeeping genes, actin and HPRT1, were examined with RT-qPCR. This was done for all 4 experiments. The graphs indicate the RGE in the different experimental set-ups (*see figure 9a-b and 10a-d*). The set-ups differ based on how long the GBM associated cells were cultivated being 3 weeks in experiment 1, 10 weeks in

experiment 2, 19 weeks in experiment 3 (both end at day 6 and end of experiment) and 23 weeks in experiment 4 (both end at day 6 and end of experiment). In experiment 1, the PBCECs exposed to U87 were significantly higher than the control and PBCECs exposed to T10 in both claudin-5 ($p < 0.05$) and VEGFR1 ($p < 0.05$). Additionally, the PBCECs exposed to U87 were significantly higher than the PBCECs exposed to T10 in P-gp in experiment 1 ($p < 0.05$).

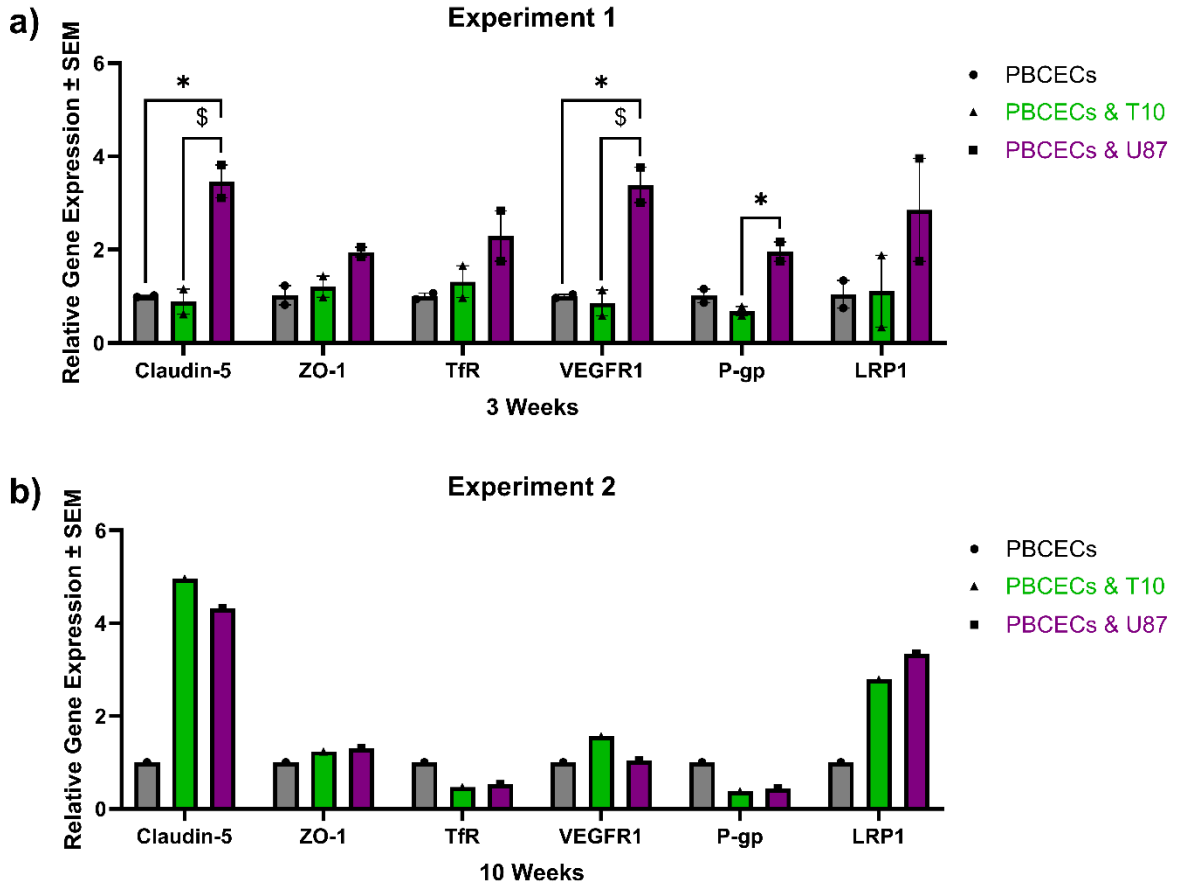

Figure 9: Relative gene expression of experiment 1 and 2. Each of the bars represents the relative mRNA expression of either claudin-5, ZO-1, TfR, VEGFR1, P-gp and LRP1 in all three of the barrier set-ups: control (grey with dot), PBCECs exposed to T10 (green with triangle) and PBCECs exposed to U87 (purple with square). * indicate the significant differences between control and PBCECs exposed to T10, whereas $ indicate the significant difference between PBCECs exposed to T10 and U87. Figure a presents the relative gene expressions of experiment 1. There is a significant difference between control (n = 2) and PBCECs exposed to U87 (n = 2) in the following genes: claudin-5 and VEGFR1. Additionally, there is a significant difference between PBCECs exposed to T10 (n = 2) and U87 in the following genes: claudin-5, VEGFR1 and P-gp. Figure b presents the relative gene expression of experiment 2. No significant differences were observed as only one RNA sample ($n = 1$) was obtained by pooling three filter inserts together for each set-up in experiment 2. All data is presented as mean ± SEM.

Experiment 3 included GBM associated cells that were cultivated for 19 weeks whereas experiment 4 included GBM associated cells that were cultivated for 23 weeks. Both experiments were combined for ending at day 6 and at the end of the experiment, respectively, to increase the statistical value. In experiments 3 and 4 combined that ended on day 6, no significant differences were observed. However, experiment 3 and 4 combined that ended at the end of the experiment showed significant increase in PBCECs exposed to U87 compared to the control in claudin-5, P-gp and LRP1 ($p < 0.05$) whereas the PBCECs exposed to T10 showed a significant increase compared to the control in claudin-5 and LRP1 ($p < 0.05$).

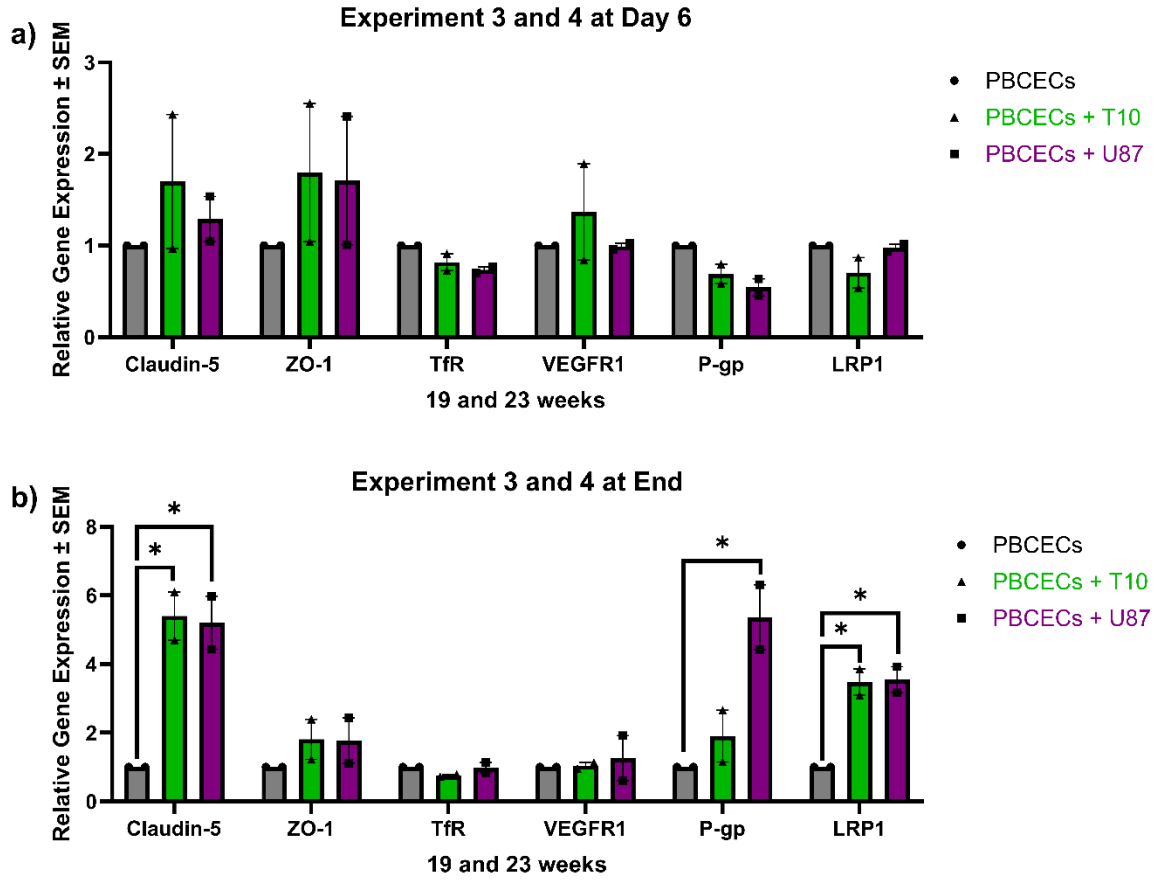

Figure 10: Relative gene expression of experiment 3 and 4 combined at day 6 and end of experiment. Each of the bars represents the relative mRNA expression of either claudin-5, ZO-1, TfR, VEGFR1, P-gp and LRP1 in all three of the barrier set-ups: control (grey with dot), PBCECs exposed to T10 (green with triangle) and PBCECs exposed to U87 (purple with square). Figure a present the relative gene expression of experiment 3 and 4 ($n = 2$), which ended on day 6. Figure b presents the relative gene expression of the end of experiment 3 and 4 ($n = 2$), which showed a significant difference between control and PBCECs exposed to T10 in claudin-5 and LRP1 and a significant difference between control and PBCECs exposed to U87 in claudin-5, P-gp and LRP1. Experiment 3 includes PBCECs exposed to T10 and U87 that were cultivated for 19 weeks whereas in experiment 4, the GBM associated cells were cultivated for 23. * indicate the significant differences between control and PBCECs exposed to GBM associated cells. All data is presented as mean ± SEM.

4.3 Gene Expression of GBM Associated Cells

RNA was obtained from both of the GBM associated cell lines, T10 and U87. As mentioned, U87 is commonly used whereas T10 is a newer cell line in GBM research. U87 is used as the control for T10. The purpose of this experiment was to investigate the RGE of the following genes, including EGFR, VEGF-A, COX-2 and Ang-2. Additionally, the expression of the housekeeping genes, actin and HPRT1, were examined with RT-qPCR. The graph indicates the RGE of U87 (control) and T10 (*see figure 11*). The GBM associated cell lines were cultivated 19 weeks prior to use in this experiment. Figure 11 shows that there is a significant decrease in T10 compared to U87 in the following genes: EGFR, VEGF-A and COX-2 ($p < 0.001$) whereas no statistical difference was observed between T10 and U87 in Ang-2.

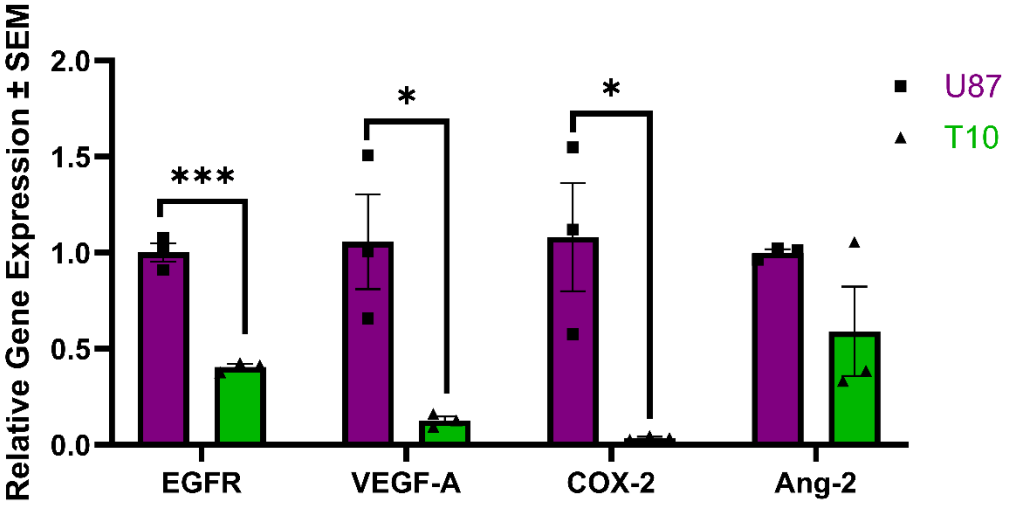

Figure 11: Relative gene expression of the GBM associated cell lines. Each bar represents the relative mRNA expression of either EGFR, VEGF-A, COX-2 and Ang-2 for both of the GBM associated cell lines, U87 (purple with square) and T10 (green with triangle). There was a significant difference between T10 (n = 3) and U87 (n = 3) in the following genes: EGFR, VEGF-A and COX-2 (***, $p < 0.001$). All data is presented as mean ± SEM.

4.4 Immunocytochemistry of Claudin-5 in BBB and BBTB models

PBCECs were cultivated in three different set-ups, including monoculture, co-culture with T10 and co-culture with U87. All three barrier models were examined for the expression of claudin-5. The staining was done for experiment 2, 3 and 4 where it included one for both at the end of day 6 and at the end of the experiment for the two last mentioned experiments.

Figure 12 shows the staining of claudin-5 from the PBCECs obtained from the three different set-ups from experiment 2, including control, co-culture with T10 and co-culture with U87. These PBCECs were stained after the end of the experiment, however, the presence of claudin-5 is unclear to assume in either of the three barrier models. Nonetheless, it can be observed that the number of nuclei varies between the models. The PBCECs exposed to T10 show a numerous number of nuclei compared to the control, but the PBCECs exposed to U87 show the least number of nuclei. Furthermore, there are indications of cell divisions on figure 12 C and F, which is specified by the white arrow.

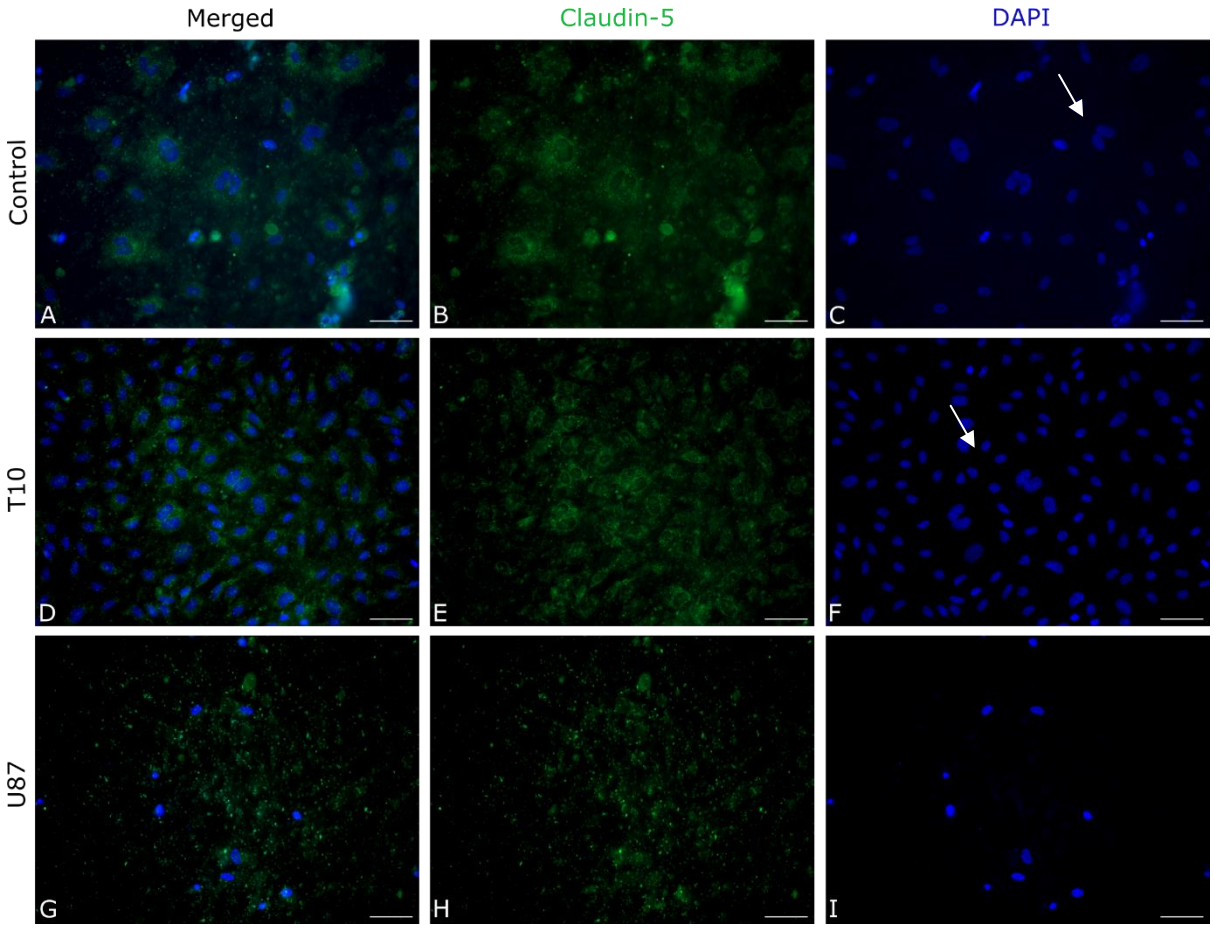

Figure 12: Immunocytochemical staining of claudin-5 in experiment 2. The figure represents the staining of claudin-5 of the PBCECs from the three barrier models, including PBCECs (control, A-C), PBCECs exposed to T10 (T10, D-F) and PBCECs exposed to U87 (U87, G-I). The GBM associated cell lines included in this staining were cultivated for 10 weeks. The PBCECs involved in this experiment were stained after the end of the experiment. The figure depicts merged images of the claudin-5 and DAPI stainings and each separately. All images were taken at 20x magnification, and the scale bars are 50 µm.

Immunocytochemical staining for claudin-5 was done for experiment 3 and 4, including the barrier models ending on day 6 and at the end of the experiment. Figures 13, 15 and 16 present the TJ structure of claudin-5 clearly, whereas it is not depicted as clearly on figure 14 in comparison. In experiment 3, the number of nuclei is visibly decreased at the end of the experiment (*see figure 14*) compared to the end at day 6 (*see figure 13*). Experiment 4, however, does not show visible difference in the number of nuclei (*see figure 15 and 16*). Throughout these experiments, cell division is a reoccurring pattern in all the stains of PBCECs exposed to GBM cells, which is indicated by white arrows. Yet, some controls also appear to go through cell division, which also is indicated by white arrows.

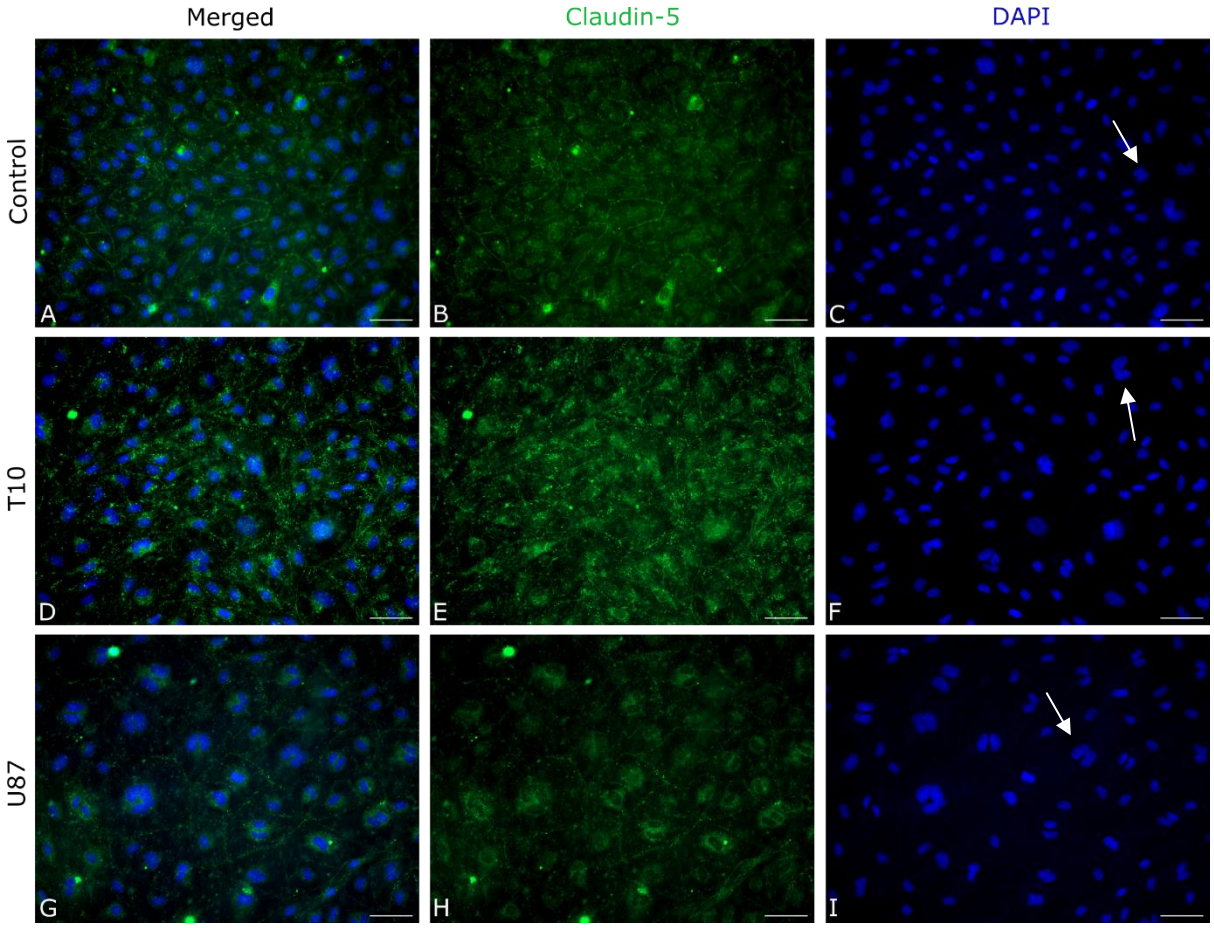

Figure 13: Immunocytochemical staining of claudin-5 in experiment 3 ending at day 6. The figure represents the staining of claudin-5 of the PBCECs from the three different barrier models, which include PBCECs (control, A-C), PBCECs exposed to T10 (T10, D-F) and PBCECs exposed to U87 (U87, G-I). The GBM associated cell lines included in this staining were cultivated for 19 weeks. The barrier models involved in this experiment ended on day 6 and stained afterwards. The figure depicts merged images of the claudin-5 and DAPI stainings and each separately. All images were taken at 20x magnification, and the scale bars are 50 µm.

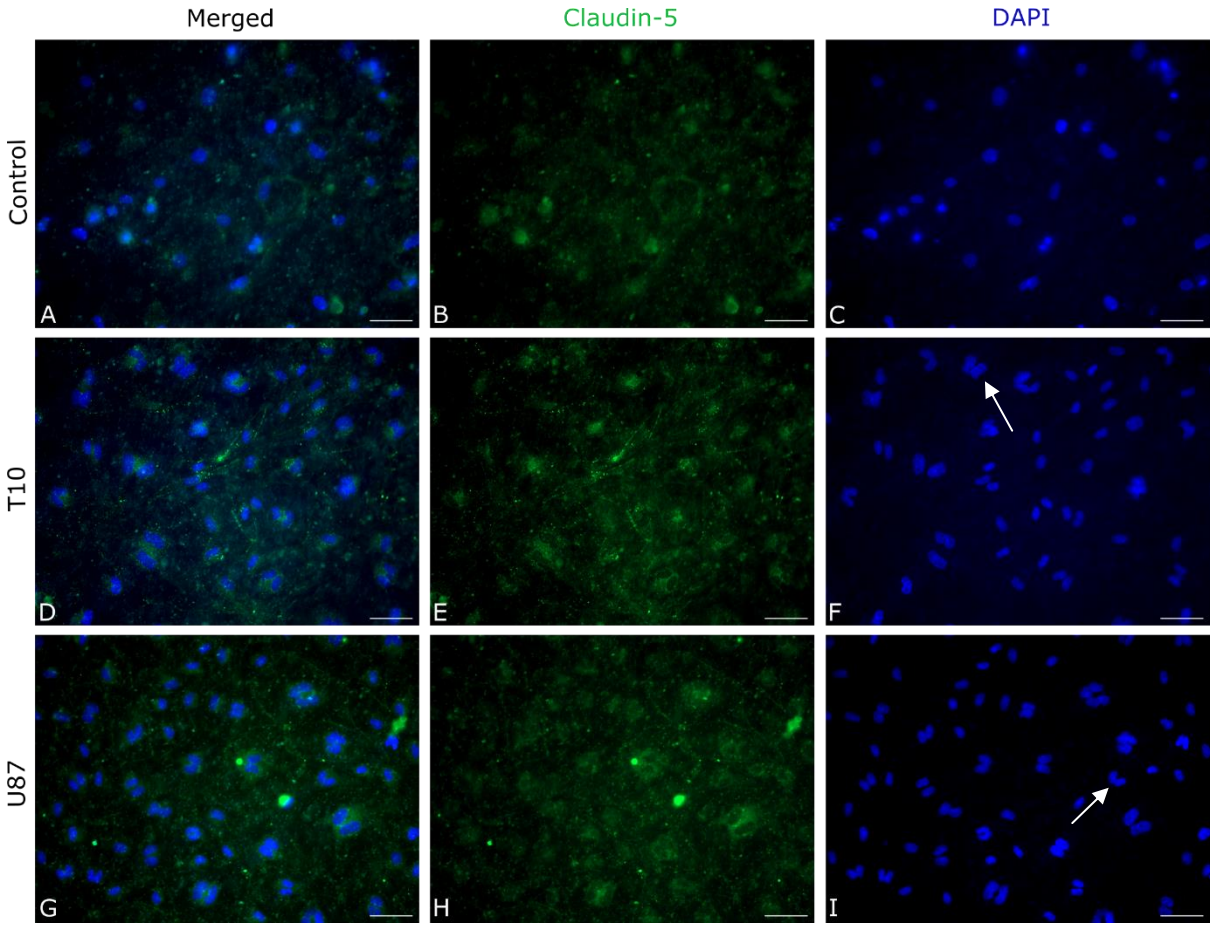

Figure 14: Immunocytochemical staining of claudin-5 in experiment 3 at the end of the experiment. The figure represents the staining of claudin-5 of the PBCECs from the three different barrier models, which include PBCECs (control, A-C), PBCECs exposed to T10 (T10, D-F) and PBCECs exposed to U87 (U87, G-I). The GBM associated cell lines included in this staining were cultivated for 19 weeks. The barrier models involved in this experiment were measured until the end of the experiment followed by staining afterwards. The figure depicts merged images of the claudin-5 and DAPI stainings and each separately. All images were taken at 20x magnification, and the scale bars are 50 µm.

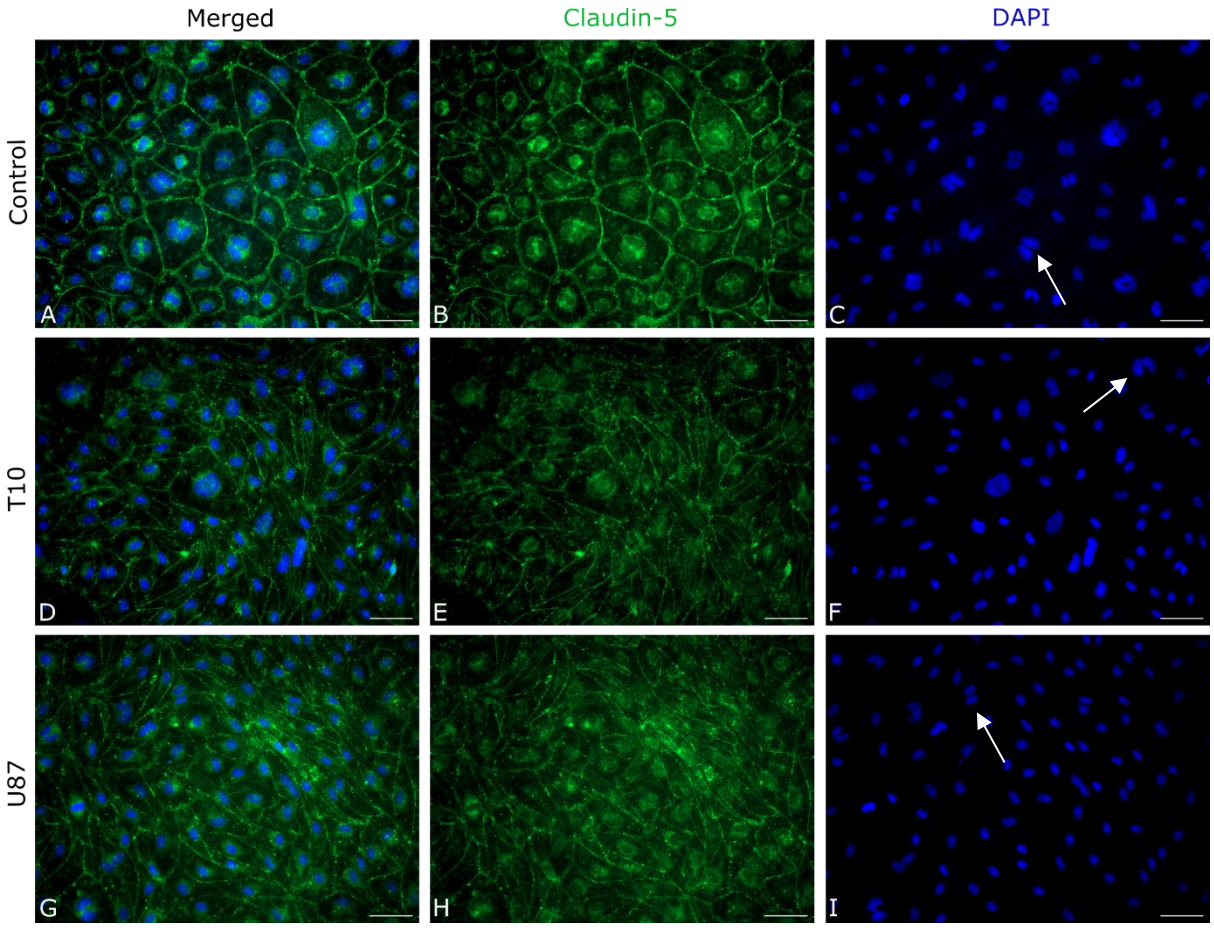

Figure 15: Immunocytochemical staining of claudin-5 in experiment 4 ending at day 6. The figure represents the staining of claudin-5 of the PBCECs from the three different barrier models, which include PBCECs (control, A-C), PBCECs exposed to T10 (T10, D-F) and PBCECs exposed to U87 (U87, G-I). The GBM associated cell lines included in this staining were cultivated for 23 weeks. The barrier models involved in this experiment ended on day 6 and stained afterwards. The figure depicts merged images of the claudin-5 and DAPI stainings and each separately. All images were taken at 20x magnification, and the scale bars are 50 µm.

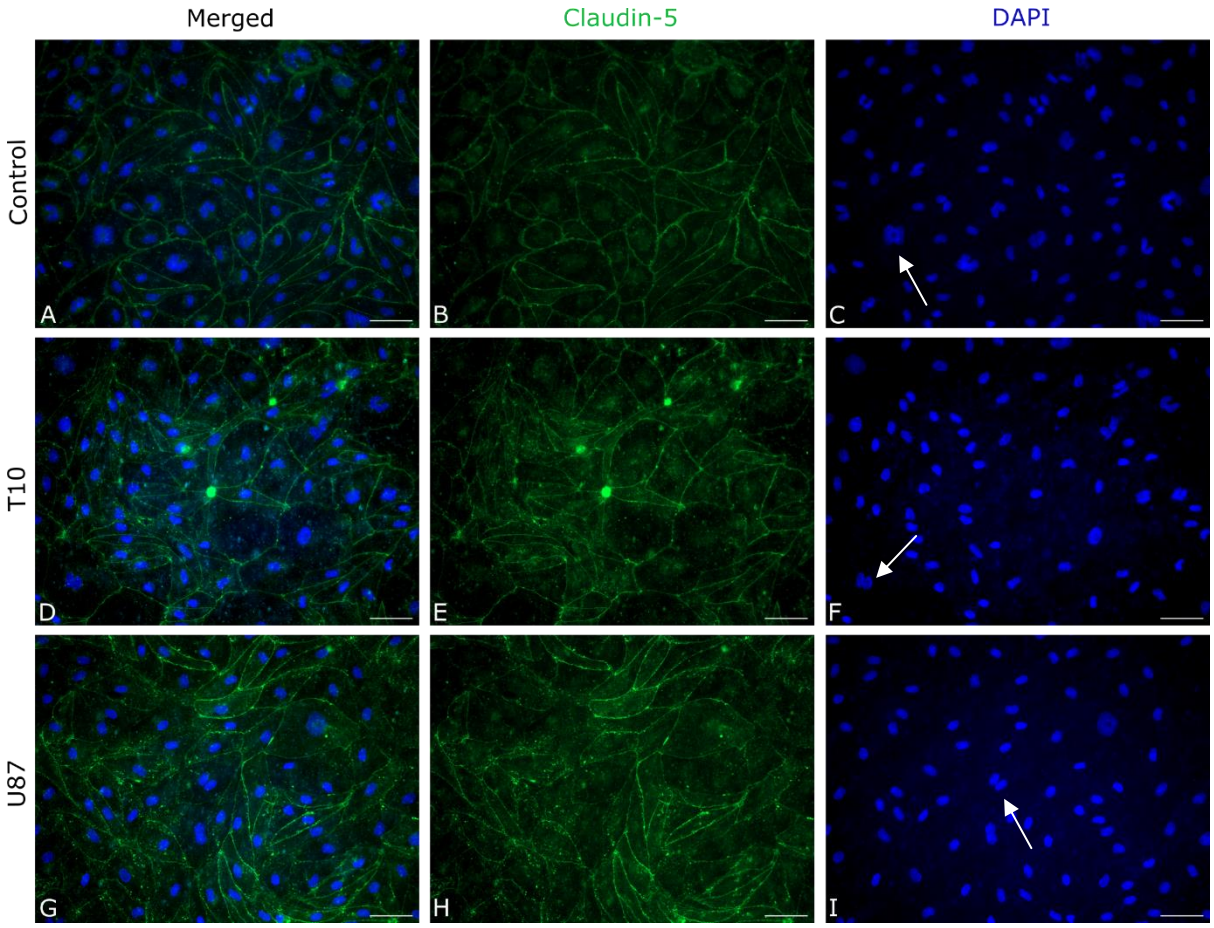

Figure 16: Immunocytochemical staining of claudin-5 in experiment 4 at the end of the experiment. The figure represents the staining of claudin-5 of the PBCECs from the three different barrier models, which include PBCECs (control, A-C), PBCECs exposed to T10 (T10, D-F) and PBCECs exposed to U87 (U87, G-I). The GBM associated cell lines included in this staining were cultivated for 23 weeks. The barrier models involved in this experiment were stained after the end of the entirety of this experiment. The figure depicts merged images of the claudin-5 and DAPI stainings and each separately. All images were taken at 20x magnification, and the scale bars are 50 µm.

4.5 Immunohistochemistry of T10

BBB disruption caused by T10 was investigated with mouse brains deposited with 300.000 T10 cells. The disruption of the BBB, which was caused by tumour growth, was investigated using staining of claudin-5, VEGFR1 and P-gp.

On the staining with claudin-5, the T10 tumour can be detected due to the darker staining of the tumour region (*see figure 17 A-F*). The tumour has reorganised the brain structure, which is indicated by the shift of the midline and asymmetrical cerebral cortex. The darker stain of the tumour (see arrows) compared to the lighter outer regions indicates an upregulation of claudin-5. This contrast between the staining can further be seen in figure 17 C and F.

The VEGFR1 stains reveal the presence of T10 tumour based on the darker outline of the tumour (*see figure 17 G-K*). The structure of the brain appears to be altered as a consequence of the tumour, which is indicated by the shifted midline and asymmetrical cerebral cortex. On figure I and L, the migration of the tumour cells can be seen, which are darker stained and appear unorganised compared to the lighter region. Contrary to the outer regions of the brain, the darker staining of the tumour indicates the upregulation of VEGFR1 (*see figure G-K*).

On figure M-R, the staining of P-gp can be seen by the darker staining where the tumour has infiltrated the corpus callosum (*see figure 17 N*) on the left section of the brain. Further the presence of the tumour cells has ventrally relocated the position of corpus callosum and caudate putamen. In comparison to the right section, the left section appears highly invaded of T10 tumour cells indicating an upregulation of P-gp.

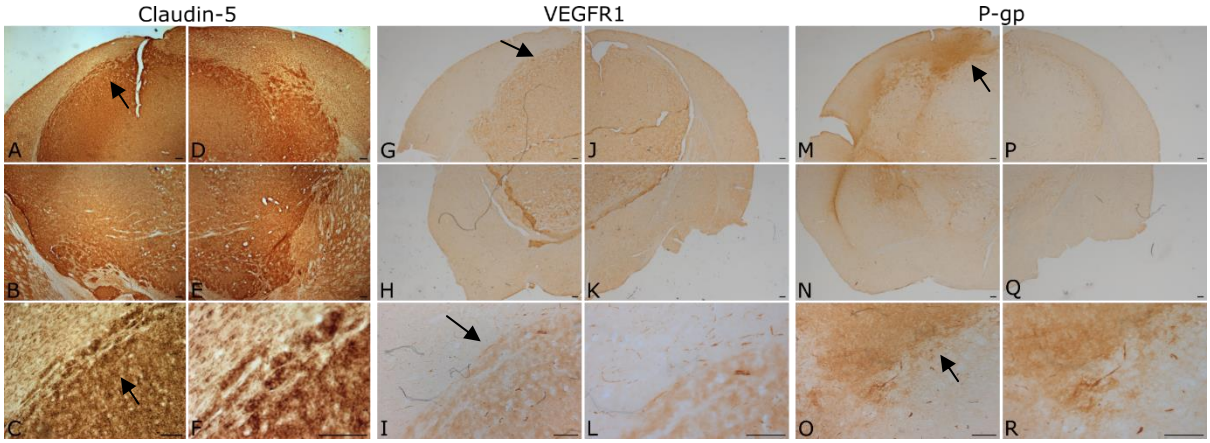

Figure 17: Immunohistochemical staining of claudin-5, VEGFR1 and P-gp. Brain sections from mice subjects deposited with 300.000 T10 cells were examined to investigate the integrity of the BBB after the development of the tumour. Figures A-F present positive staining of claudin-5, which is indicated further by arrows in figure A and C. Figures G-L shows staining of VEGFR1, which is indicated by the arrows and further with the darker stained outline around the tumour. Figure M-R presents brain parenchyma being invaded by the tumour cells leading to the loss of structure. The scale bar is set to 100 µm. All images are in the following magnifications: 2.5x (A, B, D, E, G, H, J, K, M, N, P and Q), 10x (C, I and O), 16x (L and R) and 20x (C).

5. Discussion

The integrity of the BBB is a necessity in maintaining the homeostasis of the CNS by regulating the passage of various substances between the blood and brain parenchyma. This thesis investigated the impact of the GBM associated cell lines, T10 and U87, on the integrity of BBB using PBCECs models. TEER was utilised in the investigation of permeability of the *in vitro* BBB and BBTB models where the higher TEER values indicate lower permeability and tighter junctions, resulting in a more functional and intact barrier. In addition, it was aimed to elucidate how the different GBM associated cell lines influence the BBB through RT-qPCR, with a focus on the following genes: claudin-5, ZO-1, TfR, VEGFR1, P-gp and LRP1. Further, the relative gene expression of EGFR, VEGF-A, COX-2 and Ang-2 was explored between the GBM associated cell lines, T10 and U87. Lastly, ICC and IHC were performed to investigate the integrity of the *in vitro* BBB and BBTB models for the three different set-ups and *in vivo* murine brains exposed to T10 visually, respectively.

5.1 Effects of T10 and U87 Cancer Cells on Endothelial Barrier Integrity

Across the TEER experiments conducted in this thesis, the TEER measurements indicate that the presence of T10 cells significantly enhance the integrity of the BBB when compared to control, whilst the co-culture with U87 cells was more varying from experiment to experiment.

In experiment 1 and 2, the significant increase in the observed TEER values in PBCECs exposed to T10 cells suggests that these cells may contribute to the enhancement of the barrier's integrity, contradicting with the frequent observations of cancer cells, in which GBM leads to a lower TEER value due to the secretion of soluble factors that increase the permeability of the BBB (Schneider et al., 2004). Additionally, this increase in TEER could indicate that the T10 cells may promote either the function or expression of TJs, e.g., claudin-5 and ZO-1. In contrast to the observed effects of T10 cells in experiment 1 and 2, the U87 cells did not show any significant difference over the entirety of these two experimental periods, suggesting that these cells do not instantly compromise the BBB upon interplay. However, in experiment 1, there were specific days throughout the experiment where the co-culture with U87 did show significant differences. On day 1 to 3, the co-culture with U87 significantly increased in TEER values compared to the control whereas on day 4 to 10, the TEER values significantly decreased compared to the control. This could indicate that the BBTB with U87 initially maintained the barrier's integrity

despite the presence of the aggressive GBM cells followed by a sudden decrease leading to an increase in permeability, which is commonly observed in GBM (Schneider et al., 2004).

In experiment 3 ending at day 6, the difference between the co-culture with T10 was significantly higher at the end compared to the control and co-culture with U87 whereas the co-culture with U87 was similar to the control in TEER value. This corresponds with the findings from experiment 1 and 2, indicating that T10 enhances the BBTB. However, experiment 4 ending at day 6, showed a similarity in TEER value between the co-culture with T10 and control but the co-culture with U87 showed a significant decrease in TEER values at the end of day 6 compared to the control, which aligns with previous findings of how GBM affects the BBB (Schneider et al., 2004).

Experiment 3 at the end of the experiment showed resemblance to experiment 1 and 2, as the co-culture with T10 was significantly higher than the control whereas the co-culture with U87 was not significantly higher than the control throughout the entirety of the experiment but showed significant increase at day 5 to 7 compared to the control. Experiment 4 at the end of the experiment revealed different results compared to the previous findings from this thesis. The co-culture with T10 was not significantly increased compared to the control throughout the entire experiment, however, the co-culture with U87 was significantly decreased through the overall experiment, aligning with previous findings that GBM cells secrete factors that increase the permeability of the BBB, resulting in lower TEER values (Schneider et al., 2004).

The differing effects of T10 and U87 cells on the TEER values highlight the complexity of GBM cancer cells-BBB interaction. Throughout the different experiments, the U87 cells either maintained the barrier integrity or lead to disruption of the barrier whereas the T10 cells appeared to enhance the barrier integrity. This further underscores the importance of considering the heterogeneity of the tumour cells internally and between the cell lines. Moreover, these results indicate that the BBB's response to the GBM associated cell lines is not uniform but varies from experiment to experiment, which again underlines the importance of GBM's heterogeneity. This requires further investigation to elucidate the various molecular pathways, which are involved in the GBM associated cells lines when interacting with the BBB models.

5.2 Genetic Expression of Markers in T10 and U87

To explore the GBM cell line, T10, further an RT-qPCR was performed to investigate the expression of the following genes: EGFR, VEGF-A, COX-2 and Ang-2. This relative gene expression analysis revealed that T10 expressed significantly lower amount of EGFR, VEGF-A and COX-2 compared to U87, whereas Ang-2 is decreased compared to the U87, however, it is not significant.

EGFR plays an important role in cell proliferation and survival and is particularly overexpressed in GBM, in which U87 is a commonly used GBM cell line to investigate EGFR (Stec et al., 2016, Shinojima et al., 2003). The activation of EGFR leads to the upregulation of various signaling pathways, which promote angiogenesis and invasion that further can compromise the integrity of the BBB. This would indicate that U87 would disrupt the BBB indicating lower TEER values, however, only experiment 4 till the end showed a significant difference throughout the entire experiment. Nonetheless, this could support the declining TEER values over specific times through the different TEER experiments. In contrast, the T10 cells expressed significantly lower EGFR compared to the U87 cells. This lower expression may correlate with the observed higher TEER values in the co-culture with T10, implying that the decreased EGFR signaling contributes to a less destructive interaction with the BBB. The reduced invasiveness and proliferation associated with the decreased expression of EGFR in T10 could indicate less disruption between the PBCECs, which further allows the BBB to maintain its integrity and structure.

VEGF-A is an essential gene in angiogenesis and vascular permeability, which is overexpressed in GBM cells as it promotes the formation of blood vessels, resulting in the disruption of the BBB (Plate et al., 1992). This aligns with the decreased TEER values observed in the co-culture with U87 from experiment 4 at the end, indicating that U87 expressed high levels of VEGF-A contributes to the increased permeability of the BBB. However, the T10 cells expressed a significantly decreased level of VEGF-A compared to the U87 cells, which may contribute to preserve the integrity of the BBB and thereby not decrease the TEER values of the co-culture with T10. The difference between the VEGF-A expression in T10 and U87 highlights the value of angiogenic factors in the disruption of the BBB, indicating that the T10 cells may have a less aggressive vascular nature. However, it could also indicate that U87 has developed to have a more aggressive nature as it has gone through more passages, indicating that more of the aggressive cells have been passed on to the next passage.

COX-2 plays an important role in tumour cells as it contributes to formation, growth and angiogenesis and further in inflammation (Qiu, Shi & Jiang, 2017). The U87 cells decreased the TEER values at certain timestamps in the experiment 1, 3 and 4 at the end, which could indicate increased COX-2 expression due to the exacerbation of endothelial cell stress. Contrary to U87, the T10 cells expressed significantly lower levels of COX-2, which may correlate with the observed increased TEER values in the co-culture with T10 and thereby preserving the BBB structure and function.

Lastly, Ang-2 was examined as it is involved in angiogenesis by destabilising existing blood vessels in conjunction with VEGF-A. Studies have observed that Ang-2 expression is restricted in healthy people whereas it is elevated in cancer patients (Yu, Ye, 2020). The expression of Ang-2 was neither significantly increased nor decreased in T10 compared to U87. The lack of difference between T10 and U87 could indicate that the other markers, EGFR, VEGF-A and COX-2, play a more impactful role in influencing the TEER values from the above-mentioned experiments.

The different expressions of EGFR, VEGF-A and COX-2 between T10 compared to U87 could indicate that the lower expressions in T10 contribute to a less aggressive interaction with the BBB, resulting in the integrity of the BBB.

5.3 Genetic Expression of Markers in BBB and BBTB Models

From each of the TEER experiments, RT-qPCR was performed in the three barrier models for the following markers, including claudin-5, ZO-1, TfR, VEGFR1, P-gp and LRP1, to investigate the interaction between the PBCECs and GBM associated cell lines.

5.3.1 Tight Junction Proteins – Claudin-5 and ZO-1

Claudin-5 and ZO-1 are important components to maintain the selective permeability of the BBB where their expression levels often correlate with the integrity of BBB. In experiment 1 and experiment 3 and 4 combined at the end, there was a significant increase in claudin-5 expression in the co-culture with U87 compared to the control. This may contribute to maintaining the integrity of the barrier as the TEER values of the co-culture with U87 mostly aligned with the TEER values of the control, however, there were also observed specific days throughout the experiments where the TEER values were decreased compared to the control. In addition, the PBCECs exposed to T10 showed a significant increase of claudin-5 compared to the control, which correlates with the increase of TEER values in the co-culture with T10 throughout the experiments. This could indicate that T10 promotes the stabilisation of TJs, resulting in the enhancement of the integrity of the BBB.

The findings of claudin-5 in this thesis contradict previous findings, in which the claudin-5 expression is decreased in GBM compared to control (Casili et al., 2018, Karnati et al., 2014). The lower expression of claudin-5 in GBM correlates with GBM nature in disrupting the integrity of the BBB.

No significant differences were observed in ZO-1 with the GBM cell line exposed barrier models and control. However, they were slightly increased in both of the GBM cell line exposed barrier models compared to the control in experiment 3 and 4 combined ending at day 6. The TEER values in experiment 3 and 4 ending at day 6 showed no significant difference between the barrier models. However, a study by Ishihara et al. found that there were no significant differences in the expression of ZO-1 between the control and GBM BBB model (Ishihara et al., 2008), which aligns with the results from this thesis.

5.3.2 Endothelial Function – TfR and VEGFR1

TfR plays a role in transporting iron across the BBB whereas VEGFR1 is involved in angiogenesis. Throughout the experiments, no significant difference was found between the GBM exposed barrier models compared to the control. However, a study by Ni et al. discovered an overexpression of TfR 1 in GBM in comparison to control, which the results from this thesis cannot agree or disagree with based on the results due to the RGE from the different experiments not being consistent (Ni et al., 2020). In addition, a study by Rosager et al. found that the TfR 1 increased with the malignancy grade, resulting in a significantly higher TfR 1 expression in GBM compared to control (Rosager et al., 2017).

The VEGFR1 expression was found to be significantly higher in the PBCECs exposed to U87 compared to both the control and PBCECs exposed to T10. This could further support the TEER values of T10 as the barrier is less exposed to angiogenic signalling, which could indicate that there were no significant reductions in TEER values compared to control. Despite the increase in VEGFR1 expression in the PBCECs exposed to U87, the barriers did not significantly reduce in TEER values in experiment 1, 2 and 3, which could suggest that the angiogenic signalling may not directly affect the BBB integrity. However, this aligns with the findings from experiment 4 at the end, which showed a significant decrease in TEER values compared to the control, suggesting that the elevated expression of VEGFR1 results in increased permeability in the barrier model. This last-mentioned finding correlated with existing literature, in which VEGFR1 is present in GBM but absent from BCECs (Plate et al., 1993, Atzori et al., 2018).

5.3.2 Efflux Transporters – P-gp and LRP1

P-gp is an efflux transporter at the BBB, which protects the brain by eliminating toxic substances from the brain whereas LRP1 plays an important role in maintaining homeostasis and integrity of the BBB. In experiment 1, the expression of P-gp is significantly higher in PBCECs exposed to U87 compared to PBCECs exposed to T10 cells whereas in experiment 3 and 4 combined at end, its expressed significantly higher in PBCECs exposed to U87 compared to control. A study by Abbot et al. showed that the increase of P-gp is a sign of BBB disruption, indicating that there would be a reduction in TEER values (Abbott, Rönnbäck & Hansson, 2006). However, the observations in this thesis do not have consistent TEER values corresponding to the mentioned study.

In experiment 3 and 4 combined at the end, the expression of LRP1 is significantly increased in both of the GBM exposed barrier models compared to the control. As mentioned, LRP1 is essential for preserving the BBB integrity. The elevated levels of LRP1 in both of the GBM associated cell lines could indicate that the BBB counteracts the invasiveness of GBM, suggesting increased TEER values, which can be observed in the TEER values of experiment 3 at the end but not experiment 4 at the end. Existing literature suggests that there is an increased expression of LRP1 in GBM exposed brain tissue compared to normal brain tissue (Shruthi et al., 2022), which aligns with the results of the RGE in experiment 3 and 4 combined at the end. However, the results from this thesis are not consistent throughout the different experiments.

5.4 Visualisation of Claudin-5, VEGFR1 and P-gp

In experiment 2 of the ICC staining, there is no clear visualisation of claudin-5. Experiments 3 and 4, however, show a proper visualisation of claudin-5. In experiment 3 ending at day 6, the visualisation of claudin-5 is most prominent in the control whereas in both T10 and U87 exposed PBCECs claudin-5 is present but not as continuous as in the control. Furthermore, there are more nuclei present in the control compared to the GBM exposed PBCECs, indicating there were fewer cells in the GBM associated barrier models on day 6. In experiment 3 at the end of the experiment, the visualisation of claudin-5 is more present in the GBM associated barrier models whereas in the control, it seems less present. Nonetheless, the presence of claudin-5 in the GBM associated barrier models is not continuous but more than the control. In experiment 4 ending on day 6, the presence of claudin-5 is visualised clearer in all three set-ups compared to all the set-ups from experiment 2 and 3 (both day 6 and at the end of the experiment). The merged image

indicates the presence of more claudin-5 in the GBM associated barriers compared to the control. In experiment 4 at the end, the presence of claudin-5 looks very similar in all three barrier models. An observation that was consistent in majority of the stainings was that the DAPI images highlighting the nuclei showed cell division amongst the PBCECs, however, it seems prominently increased in the GBM associated barrier models, which could indicate pro-angiogenic factors being secreted from the GBM cell lines, resulting in the mitosis of PBCECs. Existing literature shows the downregulation of claudin-5 in GBM, however, the findings in this thesis show no clear indications in downregulation of claudin-5 in the GMB associated barrier models (Karnati et al., 2014).

Further, an IHC was done to visualise claudin-5, VEGFR1 and P-gp, in which all showed a clear difference between the GBM exposed region and the non-affected region on the murine brain sections. This is indicated by the darkening of the staining of VEGFR1 and P-gp in the T10 exposed regions, which aligns with existing literature as VEGFR1 and P-gp are upregulated in association with GBM (Dréan et al., 2018, Aryal et al., 2017, Atzori et al., 2018). The section stained with claudin-5, however, showed a darker stain of the tumour region in comparison to the non-affected surrounding region, which does not associate with existing literature that indicates a downregulation of claudin-5 in GBM, resulting in the increased permeability of the BBB (Karnati et al., 2014). This staining indicates that claudin-5 is increased in T10 exposed regions, which does align with the TEER values observed for co-culture with T10 as majority showed a significant increase compared to the control.

5.5 Duration of the GBM Associated Cells in TEER Experiments

The duration of the GBM associated cells in the different TEER experiments has been a factor that could indicate the variety in some of the above-mentioned sections. The experiments have respectively involved GBM associated cancer cell lines, which have been cultivated for 3, 10, 19 and 23 weeks. An important hallmark of GBM is the heterogeneity of the cancer cells. Not only do they express variations in the different types of cancer cell lines but also within (García-Montaño et al., 2023, Boccellato, Rehm, 2022). This indicates that the prolonged cultivation of the GBM associated cell lines can lead to genetic changes and phenotypic drift, resulting in alterations of invasiveness and cell morphology (Torsvik et al., 2014). In addition, the different GBM associated cell lines can affect the BBB by secretion of factors that can change the permeability of the BBB models (García-Montaño et al., 2023). When these cells are cultured for prolonged periods, the genetic

expression of various factors, such as VEGF, may change. In this thesis, this could indicate that these changes might affect how the PBCECs interact with the GBM associated cell lines, suggesting variability in the results (Haddad et al., 2021). In experiment 3 and 4 for both ending at day 6 and at the end, the RGE were combined as it would increase the statistical value. Both of these experiments included GBM cells that were respectively cultivated for 19 and 23 weeks, which could indicate that independently each of these experiments could have each their results. This was, however, not taken into account when the data from both of the RGE were combined to increase the statistical value.

6. Conclusion

This thesis has discovered that the GBM associated cell lines, T10 and U87, each possess their unique traits and properties that affect the integrity of the BBB in different ways, resulting in variety of outcome. Alterations in the integrity of the BBB induced by T10 and U87 were observed, however, there was an increase in the TEER values of the co-culture with T10 compared to control and not a decrease. The co-culture with U87 compared to the control showed significant decrease in the TEER values at certain timestamps, which align with the aim of the thesis. The RGE observed throughout the experiments showed that the PBCECs exposed to U87 were significantly increased in claudin-5, VEGFR1, P-gp and LRP1 compared to the control. In addition, the PBCECs exposed to U87 were significantly increased in claudin-5, VEGFR1 and P-gp compared to the PBCECs exposed to T10. However, the PBCECs exposed to T10 were significantly increased in claudin-5 and LRP1 compared to the control. These results were not consistent throughout the four experiments, indicating further the importance of GBM's heterogeneity. In the ICC and IHC, the presence of claudin-5, VEGFR1 and P-gp was observed in the murine brain sections with T10, however, more murine samples are required to investigate a uniformly answer regarding the expression.

From all the findings in this thesis, it can be concluded that further investigation is required regarding GBM as its heterogeneity has an impactful role in the integrity of the BBB, resulting in different outcomes. Understanding the different characteristics of GBM and its effect on the BBB can contribute to a greater insight in treatment by enhancing the precision.

7. Bibliography

Abbott, N.J., Rönnbäck, L. & Hansson, E. 2006, "Astrocyte–endothelial interactions at the blood–brain barrier", *Nature Reviews Neuroscience,* vol. 7, no. 1, pp. 41–53.

Allen, M., Bjerke, M., Edlund, H., Nelander, S. & Westermark, B. 2016, "Origin of the U87MG glioma cell line: Good news and bad news", *Science Translational Medicine,* vol. 8, no. 354, pp. 354re3.

Amano, H., Kato, S., Ito, Y., Eshima, K., Ogawa, F., Takahashi, R., Sekiguchi, K., Tamaki, H., Sakagami, H., Shibuya, M. & Majima, M. 2015, "The Role of Vascular Endothelial Growth Factor Receptor-1 Signaling in the Recovery from Ischemia", *PloS one,* vol. 10, no. 7, pp. e0131445.

Arvanitis, C.D., Ferraro, G.B. & Jain, R.K. 2020, "The blood-brain barrier and blood-tumour barrier in brain tumours and metastases", *Nature reviews.Cancer,* vol. 20, no. 1, pp. 26–41.

Aryal, M., Fischer, K., Gentile, C., Gitto, S., Zhang, Y. & McDannold, N. 2017, "Effects on P-Glycoprotein Expression after Blood-Brain Barrier Disruption Using Focused Ultrasound and Microbubbles", *PLOS ONE,* vol. 12, no. 1, pp. e0166061.

Atzori, M.G., Tentori, L., Ruffini, F., Ceci, C., Bonanno, E., Scimeca, M., Lacal, P.M. & Graziani, G. 2018, "The Anti-Vascular Endothelial Growth Factor Receptor-1 Monoclonal Antibody D16F7 Inhibits Glioma Growth and Angiogenesis In Vivo", *The Journal of pharmacology and experimental therapeutics,* vol. 364, no. 1, pp. 77–86.

Atzori, M.G., Tentori, L., Ruffini, F., Ceci, C., Lisi, L., Bonanno, E., Scimeca, M., Eskilsson, E., Daubon, T., Miletic, H., Ricci Vitiani, L., Pallini, R., Navarra, P., Bjerkvig, R., D'Atri, S., Lacal, P.M. & Graziani, G. 2017, "The anti-vascular endothelial growth factor receptor-1 monoclonal antibody D16F7 inhibits invasiveness of human glioblastoma and glioblastoma stem cells", *Journal of experimental & clinical cancer research : CR,* vol. 36, no. 1, pp. 106–2.

Bauer, H., Krizbai, I.A., Bauer, H. & Traweger, A. 2014, "“You Shall Not Pass”—tight junctions of the blood brain barrier", *Frontiers in Neuroscience,* vol. 8.

Baumgarten, P., Blank, A., Franz, K., Hattingen, E., Dunst, M., Zeiner, P., Hoffmann, K., Bähr, O., Mäder, L., Goeppert, B., Machein, M., Seifert, V., Steinbach, J.P., Plate, K.H., Harter, P.N. & Mittelbronn, M. 2016, "Differential expression of vascular endothelial growth factor A, its receptors VEGFR-1, -2, and -3 and co-receptors neuropilin-1 and -2 does not predict bevacizumab response in human astrocytomas", *Neuro-oncology,* vol. 18, no. 2, pp. 173–183.

Belykh, E., Shaffer, K.V., Lin, C., Byvaltsev, V.A., Preul, M.C. & Chen, L. 2020, "Blood-Brain Barrier, Blood-Brain Tumor Barrier, and Fluorescence-Guided Neurosurgical Oncology: Delivering Optical Labels to Brain Tumors", *Frontiers in Oncology,* vol. 10.

Boccellato, C. & Rehm, M. 2022, "Glioblastoma, from disease understanding towards optimal cell-based in vitro models", *Cellular oncology (Dordrecht, Netherlands),* vol. 45, no. 4, pp. 527–541.

Boucher, P. & Herz, J. 2011, "Signaling through LRP1: Protection from atherosclerosis and beyond", *Biochemical pharmacology,* vol. 81, no. 1, pp. 1–5.

Boucher, Y., Salehi, H., Witwer, B., Harsh, G.R.4. & Jain, R.K. 1997, "Interstitial fluid pressure in intracranial tumours in patients and in rodents", *British journal of cancer,* vol. 75, no. 6, pp. 829–836.

Brown, L.S., Foster, C.G., Courtney, J., King, N.E., Howells, D.W. & Sutherland, B.A. 2019, "Pericytes and Neurovascular Function in the Healthy and Diseased Brain", *Frontiers in Cellular Neuroscience,* vol. 13.

Brunner, N., Stein, L., Cornelius, V., Knittel, R., Fallier-Becker, P. & Amasheh, S. 2020, "Blood-Brain Barrier Protein Claudin-5 Expressed in Paired Xenopus laevis Oocytes Mediates Cell-Cell Interaction", *Frontiers in physiology,* vol. 11, pp. 857.

Burkhart, A., Thomsen, L.B., Thomsen, M.S., Lichota, J., Fazakas, C., Krizbai, I. & Moos, T. 2015, "Transfection of brain capillary endothelial cells in primary culture with defined blood–brain barrier properties", *Fluids and Barriers of the CNS,* vol. 12, no. 1, pp. 19.

Casili, G., Caffo, M., Campolo, M., Barresi, V., Caruso, G., Cardali, S.M., Lanza, M., Mallamace, R., Filippone, A., Conti, A., Germanò, A., Cuzzocrea, S. & Esposito, E. 2018, "TLR-4/Wnt modulation as new therapeutic strategy in the treatment of glioblastomas", *Oncotarget,* vol. 9, no. 101, pp. 37564–37580.

Chai, A.B., Callaghan, R. & Gelissen, I.C. 2022, "Regulation of P-Glycoprotein in the Brain", *International journal of molecular sciences,* vol. 23, no. 23, pp. 14667. doi: 10.3390/ijms232314667.

Daneman, R. & Prat, A. 2015, "The blood-brain barrier", *Cold Spring Harbor perspectives in biology,* vol. 7, no. 1, pp. a020412.

Dolgin, E. 2016, "Venerable brain-cancer cell line faces identity crisis", *Nature,* vol. 537, no. 7619, pp. 149–150.

Dréan, A., Rosenberg, S., Lejeune, F., Goli, L., Nadaradjane, A.A., Guehennec, J., Schmitt, C., Verreault, M., Bielle, F., Mokhtari, K., Sanson, M., Carpentier, A., Delattre, J. & Idbaih, A. 2018, "ATP binding cassette (ABC) transporters: expression and clinical value in glioblastoma", *Journal of neuro-oncology,* vol. 138, no. 3, pp. 479–486.

Ehrlich, P. 1885, *Das Sauerstoff-Bedürfniss des Organismus: eine farbenanalytische Studie,* Berlin: Hirschwald.

Fischer, S., Wobben, M., Marti, H.H., Renz, D. & Schaper, W. 2002, "Hypoxia-Induced Hyperpermeability in Brain Microvessel Endothelial Cells Involves VEGF-Mediated

Changes in the Expression of Zonula Occludens-1", *Microvascular research,* vol. 63, no. 1, pp. 70–80.

García-Montaño, L.A., Licón-Muñoz, Y., Martinez, F.J., Keddari, Y.R., Ziemke, M.K., Chohan, M.O. & Piccirillo, S.G.M. 2023, "Dissecting Intra-tumor Heterogeneity in the Glioblastoma Microenvironment Using Fluorescence-Guided Multiple Sampling", *Molecular Cancer Research,* vol. 21, no. 8, pp. 755–767.

Georgieva, J.V., Hoekstra, D. & Zuhorn, I.S. 2014, "Smuggling Drugs into the Brain: An Overview of Ligands Targeting Transcytosis for Drug Delivery across the Blood-Brain Barrier", *Pharmaceutics,* vol. 6, no. 4, pp. 557–583.

Grech, N., Dalli, T., Mizzi, S., Meilak, L., Calleja, N. & Zrinzo, A. 2020, "Rising Incidence of Glioblastoma Multiforme in a Well-Defined Population", *Cureus,* .

Guo, H., Kang, H., Tong, H., Du, X., Liu, H., Tan, Y., Yang, Y., Wang, S. & Zhang, W. 2019, "Microvascular characteristics of lower-grade diffuse gliomas: investigating vessel size imaging for differentiating grades and subtypes", *European radiology,* vol. 29, no. 4, pp. 1893–1902.

Guo, X., Zhou, S., Yang, Z., Li, Z., Hu, W., Dai, L., Liang, W. & Wang, X. 2022, "Cholesterol metabolism and its implication in glioblastoma therapy", *Journal of Cancer,* vol. 13, no. 6, pp. 1745–1757.

Guo, Z., Zhang, Y., Fu, M., Zhao, L., Wang, Z., Xu, Z., Zhu, H., Lan, X., Shen, G., He, Y. & Lei, P. 2021, "The Transferrin Receptor-Directed CAR for the Therapy of Hematologic Malignancies", *Frontiers in Immunology,* vol. 12.

Haddad, A.F., Young, J.S., Amara, D., Berger, M.S., Raleigh, D.R., Aghi, M.K. & Butowski, N.A. 2021, "Mouse models of glioblastoma for the evaluation of novel therapeutic strategies", *Neuro-oncology advances,* vol. 3, no. 1, pp. vdab100.

Hanif, F., Muzaffar, K., Perveen, K., Malhi, S.M. & Simjee, S.U. 2017, "Glioblastoma Multiforme: A Review of its Epidemiology and Pathogenesis through Clinical Presentation and Treatment", *Asian Pacific journal of cancer prevention : APJCP,* vol. 18, no. 1, pp. 3–9.

Hashemi, M., Etemad, S., Rezaei, S., Ziaolhagh, S., Rajabi, R., Rahmanian, P., Abdi, S., Koohpar, Z.K., Rafiei, R., Raei, B., Ahmadi, F., Salimimoghadam, S., Aref, A.R., Zandieh, M.A., Entezari, M., Taheriazam, A. & Hushmandi, K. 2023, "Progress in targeting PTEN/PI3K/Akt axis in glioblastoma therapy: Revisiting molecular interactions", *Biomedicine & Pharmacotherapy,* vol. 158, pp. 114204.

Hervé, F., Ghinea, N. & Scherrmann, J. 2008, "CNS delivery via adsorptive transcytosis", *The AAPS journal,* vol. 10, no. 3, pp. 455–472.

Howarth, A.G., Hughes, M.R. & Stevenson, B.R. 1992, "Detection of the tight junction-associated protein ZO-1 in astrocytes and other nonepithelial cell types", *American Journal of Physiology-Cell Physiology,* vol. 262, no. 2, pp. C461–C469.

Imoukhuede, P.I. & Popel, A.S. 2012, "Expression of VEGF receptors on endothelial cells in mouse skeletal muscle", *PloS one,* vol. 7, no. 9, pp. e44791.

Ishihara, H., Kubota, H., Lindberg, R.L.P., Leppert, D., Gloor, S.M., Errede, M., Virgintino, D., Fontana, A., Yonekawa, Y. & Frei, K. 2008, "Endothelial Cell Barrier Impairment Induced by Glioblastomas and Transforming Growth Factor β2 Involves Matrix Metalloproteinases and Tight Junction Proteins", *Journal of Neuropathology & Experimental Neurology,* vol. 67, no. 5, pp. 435–448.

Jimenez-Pascual, A., Mitchell, K., Siebzehnrubl, F.A. & Lathia, J.D. 2020, "FGF2: a novel druggable target for glioblastoma?", *Expert opinion on therapeutic targets,* vol. 24, no. 4, pp. 311–318.

Johnsen, K.B., Burkhart, A., Thomsen, L.B., Andresen, T.L. & Moos, T. 2019, "Targeting the transferrin receptor for brain drug delivery", *Progress in neurobiology,* vol. 181, pp. 101665.

Jovčevska, I., Kočevar, N. & Komel, R. 2013, "Glioma and glioblastoma - how much do we (not) know?", *Molecular and clinical oncology,* vol. 1, no. 6, pp. 935–941.

Kanekiyo, T. & Bu, G. 2014, "The low-density lipoprotein receptor-related protein 1 and amyloid-β clearance in Alzheimer's disease", *Frontiers in Aging Neuroscience,* vol. 6.

Karnati, H.K., Panigrahi, M., Shaik, N.A., Greig, N.H., Bagadi, S.A.R., Kamal, M.A. & Kapalavayi, N. 2014, "Down regulated expression of Claudin-1 and Claudin-5 and up regulation of β-catenin: association with human glioma progression", *CNS & neurological disorders drug targets,* vol. 13, no. 8, pp. 1413–1426.

Kaya, M. & Ahishali, B. 2021, "Basic physiology of the blood-brain barrier in health and disease: a brief overview", *Tissue barriers,* vol. 9, no. 1, pp. 1840913.

Keaney, J. & Campbell, M. 2015, "The dynamic blood–brain barrier", *The FEBS Journal,* vol. 282, no. 21, pp. 4067–4079.

Kesari, S. 2011, "Understanding Glioblastoma Tumor Biology: The Potential to Improve Current Diagnosis and Treatments", *Seminars in oncology,* vol. 38, pp. S2–S10.

Kleihues, P., Soylemezoglu, F., Schäuble, B., Scheithauer, B.W. & Burger, P.C. 1995, "Histopathology, classification, and grading of gliomas", *Glia,* vol. 15, no. 3, pp. 211–221.

Knox, E.G., Aburto, M.R., Clarke, G., Cryan, J.F. & O'Driscoll, C.M. 2022, "The blood-brain barrier in aging and neurodegeneration", *Molecular psychiatry,* vol. 27, no. 6, pp. 2659–2673.

Koga, K., Todaka, T., Morioka, M., Hamada, J., Kai, Y., Yano, S., Okamura, A., Takakura, N., Suda, T. & Ushio, Y. 2001, "Expression of angiopoietin-2 in human glioma cells and its role for angiogenesis", *Cancer research,* vol. 61, no. 16, pp. 6248–6254.

Kwon, H.S. & Koh, S. 2020, "Neuroinflammation in neurodegenerative disorders: the roles of microglia and astrocytes", *Translational Neurodegeneration,* vol. 9, no. 1, pp. 42.

Liu, W., Wang, Z., Zhang, L., Wei, X. & Li, L. 2012, "Tight junction in blood-brain barrier: an overview of structure, regulation, and regulator substances", *CNS neuroscience & therapeutics,* vol. 18, no. 8, pp. 609–615.

Machein, M.R., Kullmer, J., Fiebich, B.L., Plate, K.H. & Warnke, P.C. 1999, "Vascular endothelial growth factor expression, vascular volume, and, capillary permeability in human brain tumors", *Neurosurgery,* vol. 44, no. 4, pp. 732–1.

Neyrinck-Leglantier, D., Lesage, J., Blacher, S., Bonnomet, A., Hunziker, W., Noël, A., Dormoy, V., Nawrocki-Raby, B., Gilles, C. & Polette, M. 2021, "ZO-1 Intracellular Localization Organizes Immune Response in Non-Small Cell Lung Cancer", *Frontiers in Cell and Developmental Biology,* vol. 9.

Ni, X., Zhao, Y., Cai, H., Yu, Z., Wang, J., Chen, F., Yu, Y., Feng, G. & Chen, Z. 2020, "Transferrin receptor 1 targeted optical imaging for identifying glioma margin in mouse models", *Journal of neuro-oncology,* vol. 148, no. 2, pp. 245–258.

Nitta, T., Hata, M., Gotoh, S., Seo, Y., Sasaki, H., Hashimoto, N., Furuse, M. & Tsukita, S. 2003, "Size-selective loosening of the blood-brain barrier in claudin-5–deficient mice", *Journal of Cell Biology,* vol. 161, no. 3, pp. 653–660.

Ohtsuki, S., Sato, S., Yamaguchi, H., Kamoi, M., Asashima, T. & Terasaki, T. 2007, "Exogenous expression of claudin-5 induces barrier properties in cultured rat brain capillary endothelial cells", *Journal of cellular physiology,* vol. 210, no. 1, pp. 81–86.

Orth, M. & Bellosta, S. 2012, "Cholesterol: its regulation and role in central nervous system disorders", *Cholesterol,* vol. 2012, pp. 292598.

Pardridge, W.M., Eisenberg, J. & Yang, J. 1987, "Human blood-brain barrier transferrin receptor", *Metabolism: clinical and experimental,* vol. 36, no. 9, pp. 892–895.

Pardridge, W.M. 2012, "Drug transport across the blood-brain barrier", *Journal of cerebral blood flow and metabolism : official journal of the International Society of Cerebral Blood Flow and Metabolism,* vol. 32, no. 11, pp. 1959–1972.

Pardridge, W.M. 2005, "The blood-brain barrier and neurotherapeutics", *NeuroRx : the journal of the American Society for Experimental NeuroTherapeutics,* vol. 2, no. 1, pp. 1–2.

Plate, K.H., Breier, G., Millauer, B., Ullrich, A. & Risau, W. 1993, "Up-regulation of vascular endothelial growth factor and its cognate receptors in a rat glioma model of tumor angiogenesis", *Cancer research,* vol. 53, no. 23, pp. 5822–5827.

Plate, K.H., Breier, G., Weich, H.A. & Risau, W. 1992, "Vascular endothelial growth factor is a potential tumour angiogenesis factor in human gliomas in vivo", *Nature,* vol. 359, no. 6398, pp. 845–848.

Profaci, C.P., Munji, R.N., Pulido, R.S. & Daneman, R. 2020, "The blood-brain barrier in health and disease: Important unanswered questions", *The Journal of experimental medicine,* vol. 217, no. 4, pp. e20190062. doi: 10.1084/jem.20190062.

Pulgar, V.M. 2019, "Transcytosis to Cross the Blood Brain Barrier, New Advancements and Challenges", *Frontiers in Neuroscience,* vol. 12.

Qiu, J., Shi, Z. & Jiang, J. 2017, "Cyclooxygenase-2 in glioblastoma multiforme", *Drug discovery today,* vol. 22, no. 1, pp. 148–156.

Rajaratnam, V., Islam, M.M., Yang, M., Slaby, R., Ramirez, H.M. & Mirza, S.P. 2020, "Glioblastoma: Pathogenesis and Current Status of Chemotherapy and Other Novel Treatments", *Cancers,* vol. 12, no. 4, pp. 937. doi: 10.3390/cancers12040937.

Rathi, S., Griffith, J.I., Zhang, W., Zhang, W., Oh, J., Talele, S., Sarkaria, J.N. & Elmquist, W.F. 2022, "The influence of the blood–brain barrier in the treatment of brain tumours", *Journal of internal medicine,* vol. 292, no. 1, pp. 3–30.

Roelofs, H.M.J., Te Morsche, R.H.M., van Heumen, B.W.H., Nagengast, F.M. & Peters, W.H.M. 2014, "Over-expression of COX-2 mRNA in colorectal cancer", *BMC gastroenterology,* vol. 14, pp. 1–1.

Rosager, A.M., Sørensen, M.D., Dahlrot, R.H., Hansen, S., Schonberg, D.L., Rich, J.N., Lathia, J.D. & Kristensen, B.W. 2017, "Transferrin receptor-1 and ferritin heavy and light chains in astrocytic brain tumors: Expression and prognostic value", *PLOS ONE,* vol. 12, no. 8, pp. e0182954.

Schlageter, K.E., Molnar, P., Lapin, G.D. & Groothuis, D.R. 1999, "Microvessel organization and structure in experimental brain tumors: microvessel populations with distinctive structural and functional properties", *Microvascular research,* vol. 58, no. 3, pp. 312–328.

Schneider, S.W., Ludwig, T., Tatenhorst, L., Braune, S., Oberleithner, H., Senner, V. & Paulus, W. 2004, "Glioblastoma cells release factors that disrupt blood-brain barrier features", *Acta Neuropathologica,* vol. 107, no. 3, pp. 272–276.

Seker-Polat, F., Pinarbasi Degirmenci, N., Solaroglu, I. & Bagci-Onder, T. 2022, "Tumor Cell Infiltration into the Brain in Glioblastoma: From Mechanisms to Clinical Perspectives", *Cancers,* vol. 14, no. 2, pp. 443. doi: 10.3390/cancers14020443.

Sharma, P., Aaroe, A., Liang, J. & Puduvalli, V.K. 2023, "Tumor microenvironment in glioblastoma: Current and emerging concepts", *Neuro-oncology advances,* vol. 5, no. 1, pp. vdad009.

Shinojima, N., Tada, K., Shiraishi, S., Kamiryo, T., Kochi, M., Nakamura, H., Makino, K., Saya, H., Hirano, H., Kuratsu, J., Oka, K., Ishimaru, Y. & Ushio, Y. 2003, "Prognostic value of epidermal growth factor receptor in patients with glioblastoma multiforme", *Cancer research,* vol. 63, no. 20, pp. 6962–6970.

Shruthi, N.R., Behera, M.M., Naik, S.K., Das, S.K., Gopan, S., Ghosh, A., Sahu, R.N., Patra, S. & Purkait, S. 2022, "Elevated expression of cholesterol transporter LRP-1 is crucially implicated in the pathobiology of glioblastoma", *Frontiers in Neurology,* vol. 13.

Song, J., Lu, C., Leszek, J. & Zhang, J. 2021, "Design and Development of Nanomaterial-Based Drug Carriers to Overcome the Blood-Brain Barrier by Using Different Transport Mechanisms", *International journal of molecular sciences,* vol. 22, no. 18, pp. 10118. doi: 10.3390/ijms221810118.

Stec, W.J., Rosiak, K., Siejka, P., Peciak, J., Popeda, M., Banaszczyk, M., Pawlowska, R., Treda, C., Hulas-Bigoszewska, K., Piaskowski, S., Stoczynska-Fidelus, E. & Rieske, P. 2016, "Cell line with endogenous EGFRvIII expression is a suitable model for research and drug development purposes", *Oncotarget,* vol. 7, no. 22, pp. 31907–31925.

Stevenson, B.R., Siliciano, J.D., Mooseker, M.S. & Goodenough, D.A. 1986, "Identification of ZO-1: a high molecular weight polypeptide associated with the tight junction (zonula occludens) in a variety of epithelia", *The Journal of cell biology,* vol. 103, no. 3, pp. 755–766.

Sweeney, M.D., Zhao, Z., Montagne, A., Nelson, A.R. & Zlokovic, B.V. 2019, "Blood-Brain Barrier: From Physiology to Disease and Back", *Physiological Reviews,* vol. 99, no. 1, pp. 21–78.

Thomsen, L.B., Burkhart, A. & Moos, T. 2015, "A Triple Culture Model of the Blood-Brain Barrier Using Porcine Brain Endothelial cells, Astrocytes and Pericytes", *PloS one,* vol. 10, no. 8, pp. e0134765.

Thomsen, M.S., Humle, N., Hede, E., Moos, T., Burkhart, A. & Thomsen, L.B. 2021, "The blood-brain barrier studied in vitro across species", *PloS one,* vol. 16, no. 3, pp. e0236770.

Torsvik, A., Stieber, D., Enger, P.Ø, Golebiewska, A., Molven, A., Svendsen, A., Westermark, B., Niclou, S.P., Olsen, T.K., Chekenya Enger, M. & Bjerkvig, R. 2014, "U-251 revisited: genetic drift and phenotypic consequences of long-term cultures of glioblastoma cells", *Cancer medicine,* vol. 3, no. 4, pp. 812–824.

Toyoda, K., Tanaka, K., Nakagawa, S., Thuy, D.H.D., Ujifuku, K., Kamada, K., Hayashi, K., Matsuo, T., Nagata, I. & Niwa, M. 2013, "Initial contact of glioblastoma cells with existing normal brain endothelial cells strengthen the barrier function via fibroblast growth factor 2 secretion: a new in vitro blood-brain barrier model", *Cellular and molecular neurobiology,* vol. 33, no. 4, pp. 489–501.

van Assema, D.M.E., Lubberink, M., Boellaard, R., Schuit, R.C., Windhorst, A.D., Scheltens, P., Lammertsma, A.A. & van Berckel, B.N.M. 2012, "P-glycoprotein function at the blood-brain barrier: effects of age and gender", *Molecular imaging and biology,* vol. 14, no. 6, pp. 771–776.

van Tellingen, O., Yetkin-Arik, B., de Gooijer, M.C., Wesseling, P., Wurdinger, T. & de Vries, H.E. 2015, "Overcoming the blood–brain tumor barrier for effective glioblastoma treatment", *Drug Resistance Updates,* vol. 19, pp. 1–12.

Wu, D., Chen, Q., Chen, X., Han, F., Chen, Z. & Wang, Y. 2023, "The blood–brain barrier: structure, regulation, and drug delivery", *Signal Transduction and Targeted Therapy,* vol. 8, no. 1, pp. 217.

Wu, W., Klockow, J.L., Zhang, M., Lafortune, F., Chang, E., Jin, L., Wu, Y. & Daldrup-Link, H.E. 2021, "Glioblastoma multiforme (GBM): An overview of current therapies and mechanisms of resistance", *Pharmacological research,* vol. 171, pp. 105780.

Xing, P., Liao, Z., Ren, Z., Zhao, J., Song, F., Wang, G., Chen, K. & Yang, J. 2016, "Roles of low-density lipoprotein receptor-related protein 1 in tumors", *Chinese journal of cancer,* vol. 35, pp. 6–0.

Yu, X. & Ye, F. 2020, "Role of Angiopoietins in Development of Cancer and Neoplasia Associated with Viral Infection", *Cells,* vol. 9, no. 2, pp. 457. doi: 10.3390/cells9020457.

Zhang, X., Wang, L., Zhang, H., Tu, F., Qiang, Y. & Nie, C. 2019, "Decreased expression of ZO-1 is associated with tumor metastases in liver cancer", *Oncology letters,* vol. 17, no. 2, pp. 1859–1864.

Zhang, Y., Dube, C., Gibert, M.J., Cruickshanks, N., Wang, B., Coughlan, M., Yang, Y., Setiady, I., Deveau, C., Saoud, K., Grello, C., Oxford, M., Yuan, F. & Abounader, R. 2018, "The p53 Pathway in Glioblastoma", *Cancers,* vol. 10, no. 9, pp. 297. doi: 10.3390/cancers10090297.

Zhao, Y., Li, D., Zhao, J., Song, J. & Zhao, Y. 2016, "The role of the low-density lipoprotein receptor-related protein 1 (LRP-1) in regulating blood-brain barrier integrity", *Reviews in the neurosciences,* vol. 27, no. 6, pp. 623–634.